High-Field Studies of Band Ferromagnetism in Fe and Ni by Mössbauer and Magnetic Moment Measurements

S. FONER
Francis Bitter National Magnet Laboratory, Massachusetts Institute of Technology, Cambridge, Massachusetts 02139*

AND

A. J. FREEMAN†‡
Francis Bitter National Magnet Laboratory, Massachusetts Institute of Technology, Cambridge, Massachusetts 02139*
and
Department of Physics, Northwestern University, Evanston, Illinois 62201

AND

N. A. BLUM
Francis Bitter National Magnet Laboratory, Massachusetts Institute of Technology, Cambridge, Massachusetts 02139*
and
National Aeronautics and Space Administration, Electronics Research Center, Cambridge, Massachusetts 02139

AND

R. B. FRANKEL, E. J. MCNIFF, JR., AND H. C. PRADDAUDE
Francis Bitter National Magnet Laboratory, Massachusetts Institute of Technology, Cambridge, Massachusetts 02139*

(Received 13 December 1968)

High-field susceptibility χ_{HF} in Fe and Ni (at 4.2, 77, and 300°K) and high-field Mössbauer studies in Fe at 4.2°K are reported and related to the band structure of Fe and Ni and to band models of ferromagnetism. The Mössbauer effect was employed to measure the change in the hyperfine field H_n at the ^{57}Fe nucleus with application of an external field. Assuming H_n to be proportional to the bulk magnetization, a microscopic equivalent to χ_{HF} is obtained. We also show how the high-field data may be used alternatively to determine the nuclear g factor. The macroscopic differential magnetic moment measurements are presented along with an extensive discussion of the experiments to 150 kG. We find $\chi_{HF}=4.3\times10^{-5}$ emu/cc for Fe and 1.7×10^{-5} emu/cc for Ni at 4.2°K, where χ_{HF} is averaged from 50–150 kG. The interpretation of these low-temperature data (when reasonable estimates of Van Vleck susceptibility are made) indicates holes in both spin bands of Fe and a full band of one spin in N, in agreement with the accepted band theory picture for these metals and with recent spin-polarized and pseudopotential band calculations for magnetic Fe and Ni. The differential magnetic moment measurements at higher temperatures are in reasonable agreement with predictions of spin-wave theory. In the Appendices we include: (a) a tabulation of the field-dependent terms which enter into the spin-wave description of the magnetization and their derivatives with respect to field and temperature, (b) a discussion of depolarization effects and their influence on the approach to saturation, and (c) a discussion of the dependence of the magnetic moment measurements on sample positioning errors.

I. INTRODUCTION

TWO models for ferromagnetism have been discussed for many years—the localized model and the band or collective (itinerant) electron model.[1] Although it might appear that these two disparate models should lead to quite different magnetic properties of a solid, this is not the case. For instance, the temperature dependence of the magnetic moment in Fe and Ni can be described by spin-wave models,[2,3] but spin waves may equally well be described by either localized or band electrons—as first discussed by Herring and Kittel.[4] Although differences are predicted by the collective models,[1,5] in general, there are few experiments which permit a clear distinction between the localized and the itinerant models and these experiments are difficult to perform with sufficient resolution. Wohlfarth[5] has pointed out that the high-field behavior of the magnetic moment leads to clear distinctions between these two models. When both (up and down) partially occupied spin bands are involved we expect a finite magnetic

* Supported by the U. S. Air Force Office of Scientific Research.
† Supported in part by the U. S. Advanced Research Projects Agency through the Northwestern University Material Science Center.
‡ Permanent address: Department of Physics, Northwestern University, Evanston, Ill.

[1] C. Herring, in *Magnetism*, edited by G. T. Rado and H. Suhl (Academic Press Inc., New York, 1966), Vol. 4 and extensive references therein.

[2] B. E. Argyle, S. H. Charap, and E. W. Pugh, Phys. Rev. **132**, 2051 (1963), and references cited therein.

[3] F. Keffer, in *Handbuch der Physik*, edited by H. P. J. Wijn (Springer-Verlag, Berlin, 1966), Vol. 18, p. 2.

[4] C. Herring and C. Kittel, Phys. Rev. **81**, 869 (1951).

[5] E. P. Wohlfarth, Phys. Letters **3**, 17 (1962).

susceptibility ($\chi_{HF}=\partial M/\partial H>0$ well above technical saturation), even when sufficiently low temperatures and high fields completely suppress spin-wave contributions. In contrast, the localized models predict complete saturations, so that $\chi_{HF}=0$ under the same circumstances.

The high-field magnetic susceptibility in Fe and Ni and high-field Mössbauer studies in Fe are examined in this paper and related to the band structure of Fe and Ni and band models of ferromagnetism. The measurements at 4.2°K in Fe present clear evidence favoring the collective-electron model, and both the Fe and Ni experiments provide information regarding the magnetic band structure in these metals. The magnetic-moment measurements at higher temperatures are compared with predictions of spin-wave theory. The differential magnetization measurements reported here are an extension of earlier studies reported briefly[6] and were continued in order to resolve an apparent controversy with other[7] (lower-field) data. The reasons for these differences in experimental results are examined and clarified; we show that our previous conclusions remain valid. Since our earlier work, pulsed-field data to 200 kG have been reported[8] which corroborate our results as well as the more detailed studies presented in this paper. Recent spin-polarized[9,10] and pseudopotential[11] band calculations for magnetic Fe and Ni also are consistent with our results.

As emphasized by Wohlfarth[5] and discussed recently by Herring,[1] the collective electron theory of ferromagnetism predicts a relative magnetization at absolute zero ζ_0 which may be less than unity depending on details of the density of states in the metal at the Fermi energy $N(\epsilon_F)$ and the strength of the Weiss molecular field. For example, it has generally been assumed in the collective electron picture that Ni is a "strong" ferromagnet ($\zeta_0=1$) and the Fe is a "weak" ferromagnet ($\zeta_0<1$). This terminology is confusing: A weak ferromagnet is one in which the internal (exchange) field is not capable of completely polarizing one of the spin bands against one-electron depolarization effects. Thus, the application of an intense external magnetic field should cause, at very low temperatures, an increase in ζ_0 if ζ_0 is indeed less than 1. Such an increase in ζ_0 is incompatible, however, with theories based on entirely localized atomic moments which require $\zeta_0\equiv 1$ at $T=0$°K.

This difference may be seen if one looks at the high-field band susceptibility χ_d which (at $T=0$°K) from the collective electron theory is given by

$$n\mu_B^2/\chi_d=\tfrac{1}{4}n[1/N(\epsilon_{F\uparrow})+1/N(\epsilon_{F\downarrow})]-k\theta'. \quad (1)$$

In writing Eq. (1), we ignore VanVleck paramagnetism, spin-wave, and other contributions to the total susceptibility χ. (These contributions are discussed in detail later in this paper.) Equation (1) is a consequence of simple collective electron theory where we assume that the total energy is the sum of single-particle (band-state) energies (i.e., the Hartree approximation) and an exchange energy contribution which raises (lowers) the down (up)-spin bands relative to the up (down)-spin bands. In the expression for χ_d, n is the total number of electrons, $N(\epsilon_{F\uparrow})$ and $N(\epsilon_{F\downarrow})$ are the up- and down-spin densities of states at the Fermi energy, respectively, and $k\theta'$ is the molecular field represented by a characteristic temperature θ' and is proportional to the exchange splitting of the different spin bands. It is clear that if $\zeta_0=1$, $\chi_d=0$, since $N(\epsilon_{F\uparrow})$ or $N(\epsilon_{F\downarrow})=0$; on the other hand, if neither $N(\epsilon_{F\uparrow})$ nor $N(\epsilon_{F\downarrow})=0$, then $\chi_d>0$. Thus the measurements of χ will yield a value for χ_d (provided the other contributions to χ can be determined) which may be used to obtain information about the occupancy of the spin bands.

One purpose of this paper is to report in detail new measurements of χ_{HF} for Ni and Fe over a range of temperatures. Section II describes and discusses the Mössbauer effect measurements of the change in the hyperfine field H_{int}, at the ^{57}Fe nucleus. Assuming H_{int} to be proportional to the bulk magnetization, a microscopic equivalent to χ_{HF} is obtained. We also show how the high-field data may be used to determine the nuclear g factors. The macroscopic differential magnetic moment measurements are presented in Sec. III along with an extensive discussion of the experimental conditions and difficulties involved in carrying out such experiments both in high-field Bitter magnets and in superconducting magnets. The Mössbauer and the magnetization results are discussed in Sec. IV. An interpretation of the low-temperature results is given based on collective electron theory and compared with the predictions of recent energy-band calculations. The high-temperature data are compared with spin-wave predictions. In Sec. V we examine possible sources of a field-dependent χ_{HF}. Finally, in Sec. VI some of our conclusions are summarized. Appendix A works out the corrections required to account for small depolarizing effects which are extremely important in the lower-field range for non-ellipsoidal samples. In Appendix B we examine the effects of small sample positioning errors in the detection coil system. The field-dependent terms which enter into the spin-wave description of the magnetization are tabulated in Appendix C as are their derivatives with respect to field and temperature for selected ranges.

[6] A. J. Freeman, N. A. Blum, S. Foner, R. B. Frankel, and E. J. McNiff, Jr., J. Appl. Phys. **37**, 1338 (1966).
[7] C. Herring, R. M. Bozorth, A. E. Clark, and T. R. McGuire, J. Appl. Phys. **37**, 1340 (1966).
[8] J. H. M. Stoelinga and R. Gersdorf, Phys. Letters **19**, 640 (1966); J. H. M. Stoelinga, thesis, University of Amsterdam, 1967 (unpublished).
[9] S. Wakoh and J. Yamashita, J. Phys. Soc. (Japan) **21**, 1712 (1966).
[10] J. W. D. Connolly, Phys. Rev. **159**, 415 (1967); and (to be published).
[11] L. Hodges, H. Ehrenreich, and N. D. Lang, Phys. Rev. **152**, 505 (1966); L. Hodges and H. Ehrenreich, J. Appl. Phys. **39**, 1280 (1968).

For consistency throughout this paper we refer to "the magnetic field *in vacuo*" as H (with various subscripts) and measure it in units of gauss. In some instances it would have been more appropriate to use the magnetic induction B such as when referring to the "field" at the center of a solenoid. (We employ H_0 as the applied magnetic field). In this way we avoid equations containing both H and B and mixed units of gauss and oersted when the permeability of the medium is identically unity. Whenever the permeability of the medium is not unity, we use H or B explicitly as appropriate to the discussion at hand.

II. MÖSSBAUER STUDIES

A. Hyperfine Field in Ferromagnets

The Mössbauer technique may be used to investigate directly the change of the Fe hyperfine field with applied magnetic field. If we *assume* that the bulk magnetization is proportional to the moment localized on each iron atom and that the internal hyperfine field is proportional to the latter (after allowing for the applied field and the demagnetizing field) *then* the magnetization and Mössbauer measurements should give equivalent results within their respective limits of error.

Let us consider this proportionality in detail and consider the origin[12] of the hyperfine field H_{int}, measured at nuclei in ferromagnets, although this is still not fully understood. The total hyperfine field H_{int} equal to -340 kG in iron metal at 0°K, is thought to arise from the following sources:

(i) A "local" field consisting of demagnetizing and Lorentz fields H_{DM}.

(ii) An electronic orbital contribution arising from any unquenched orbital angular momentum. In Fe this contribution amounts to about 10 kG.

(iii) An electronic spin-dipole contribution from surrounding ions. In cubic systems this term is identically zero. Although magnetostriction destroys the cubic symmetry, the forced magnetostriction above saturation yields a negligible contribution[13] to H_{int}.

(iv) The negative field arising via the Fermi contact term which is due to polarization of the core s electrons H_c.

(v) A contact field H_s from polarized conduction electrons which have s character and hence a nonzero spin density at the nucleus. For iron this is thought to amount to about $+100$ kG.

(vi) A positive contact field from s-like conduction electrons admixed into the partially filled magnetic $3d$ bands. This term is positive because there are more up-spin than down-spin electrons.

(vii) A negative contact field from s-like conduction electrons covalently admixed into the open $3d$ bands. This term is negative because there are more holes in the down-spin than in the up-spin band.

One considers H_c, term (iv), to be the dominant contribution to H_{int} since crude perturbation estimates have indicated that terms (vi) and (vii) tend to cancel.[14] The core field H_c must equal the observed field H_{int} (-340 kG) minus the field H_s ($+100$ kG). Although this value for H_c is larger than expected from free-ion calculations,[12] it appears reasonable for a solid if one considers the effect of an expanded (or contracted) $3d$-charge density as was shown by Freeman and Watson.[15]

The magnetization M is essentially made up of the same terms as those listed above for the hyperfine field. Since the two dominant terms [(iv) and (v) above] are each proportional to $\langle S_z \rangle$, and since we neglect the other small contributions to H_{int}, we assume M to be proportional to $\langle S_z \rangle$ also and so argue that $H_{\text{int}} \propto M$. Here it should be emphasized that although many of the neglected contributions are small, or may cancel each other, this does not assure us that the differential changes of these quantities with H are small, or even of the same sign. In considering the change in H_{int} with applied field, it is not strictly correct to set this change proportional to ΔM. While term (ii) above makes only a small contribution to H_{int} the orbital or Van Vleck paramagnetism results in one of the largest contributions to the Knight shift, i.e., the change in the hyperfine field with applied field. The orbital Knight shift term K_{VV}, may be shown to be about 0.2% for metallic ion; this is within the limit of our experimental error. The Van Vleck susceptibility is discussed more fully in Sec. IV. Unlike the different contributions to χ which are of the same sign for the dominant terms, the Knight shift contributions are of opposite sign. As we shall see, for the small quantities involved, there may be additional terms not even enumerated here. A comparison of χ_{HF} with $\Delta H_{\text{int}}/\Delta H_0$ demonstrates that there appears to be a cancellation of such effects so that the assumption H_{int} proportional to M appears justified within the accuracy of the present Mössbauer experiments.

B. Experimental Determination of H_n

The Mössbauer effect in metallic iron has been studied extensively.[16–18] The salient features of the usual velocity spectrum obtained by measuring the

[12] A. J. Freeman and R. E. Watson, in *Magnetism*, edited by G. T. Rado and H. Suhl (Academic Press, Inc., New York, 1965), Vol. IIA, p. 167; R. E. Watson and A. J. Freeman, in *Hyperfine Interactions*, edited by A. J. Freeman and R. B. Frankel (Academic Press Inc., New York, 1967), p. 53.

[13] E. Fawcett and G. K. White, J. Appl. Phys. **38**, 1320 (1967).

[14] P. W. Anderson and A. M. Clogston, Bull. Am. Phys. Soc. **2**, 124 (1961).

[15] A. J. Freeman and R. E. Watson, Phys. Rev. Letters **5**, 498 (1960).

[16] H. Frauenfelder, *The Mössbauer Effect* (W. A. Benjamin, Inc., New York, 1962).

[17] R. S. Preston, S. S. Hanna, and J. Heberle, Phys. Rev. **128**, 2207 (1962).

[18] N. A. Blum and L. Grodzins, Phys. Rev. **136**, A133 (1964).

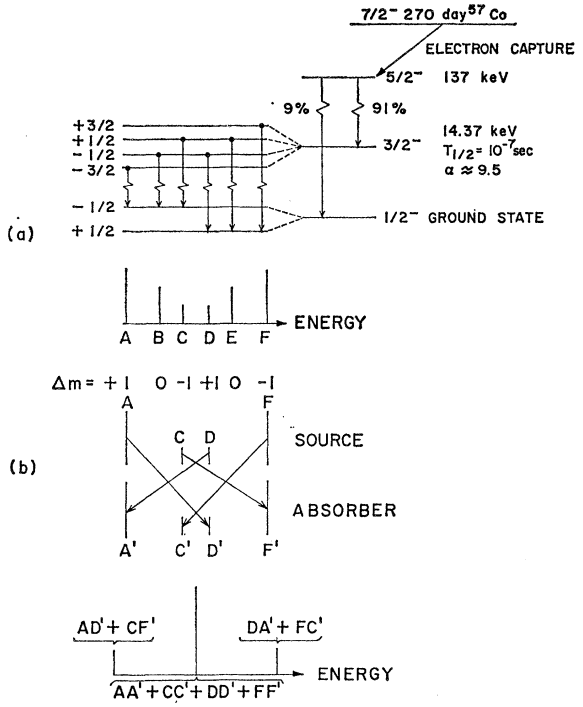

FIG. 1. (a) Decay scheme of ^{57}Co and the magnetic hyperfine structure of the 14.4-keV transition of ^{57}Fe giving a six-line absorption spectrum for an unpolarized iron foil absorber and a single-line source. The relative intensity is indicated by the height of the absorption lines. (b) Absorption spectrum obtained when both source and absorber levels are split by parallel longitudinal hyperfine fields of the same magnitude. The Doppler shift displaces the source energy levels relative to those of the absorber so that the overlap produces the three resonance lines shown.

resonance absorption of 14.4-keV γ-rays from a single-line source containing ^{57}Co by a metallic iron absorber are as follows:

(1) A six-line magnetic-hyperfine spectrum is obtained corresponding to the six allowed $\Delta m=\pm 1,0$ magnetic dipole transitions from the 14.4-keV, $I=\frac{3}{2}$ nuclear levels to the ground state, $I=\frac{1}{2}$ nuclear levels in ^{57}Fe [cf. Fig. 1(a)].

(2) The relative intensities of the lines (for a thin absorber) are

$$\alpha: I_1=I_6=3(1+\cos^2\theta),$$
$$\beta: I_2=I_5=4\sin^2\theta,$$
$$\gamma: I_3=I_4=1+\cos^2\theta,$$

where the subscripts 1–6 correspond to resonance lines increasing in energy, and where θ is the angle between the (net) magnetic field acting at the ^{57}Fe nucleus and the γ-ray propagation direction. The intensity ratios thus give information concerning the relative direction of the hyperfine field.

(3) The magnitudes of the splittings between the various pairs of lines yield only the ratio of the excited and ground-state g factors (the corresponding moments are $g_i I_i \mu_N$ (the subscript $i=1$ for the excited state, and 0 for the ground state),

$$g_1/g_0=(v_1-v_2)/(v_2+v_3), \tag{2}$$

where v_1 is the splitting between lines 1 and 6, v_2 the splitting between lines 2 and 5 and v_3 the splitting between lines 3 and 4 in any units (cf. Fig. 1). The ratio of the moments, $\mu_1/\mu_0=-3g_1/g_0$, is found to be[17] -1.715 ± 0.004. The ground-state moment has been obtained from double resonance experiments so that the value of the total hyperfine field acting at the nucleus may be found from the splitting between any pair of resonance lines; e.g., $H_n=v_1[E_0/(3g_1+g_0)\mu_N c]$, where E_0 is the γ-ray energy, μ_N is the nuclear magneton, and c is the velocity of light. The factor in the parentheses is a constant for a given nuclear transition; the total hyperfine field in the ^{57}Fe hyperfine spectrum is $H_n=30.96v_1$ kG, where v_1 is measured in mm/sec.

In the particular case where identical hyperfine fields act on both the source nuclei and the absorber nuclei and where the directions of the hyperfine fields are parallel to each other and collinear with the γ-ray propagation direction, it has been shown[18] that a three-line velocity spectrum is obtained [cf. Fig. 1(b)] and that the value of the hyperfine field is

$$H_n=v[E_0/2(g_0+g_1)\mu_N c], \tag{3}$$

where v is the splitting between the outer lines of the spectrum; if v is measured in mm/sec, the hyperfine field is $H_n=26.76v$ kG.

It is possible that the ground and excited nuclear levels are not split by the same effective magnetic field. This effect is related to the hyperfine structure anomaly[19,20] which is sensitive to the distribution of the magnetic field within the volume occupied by the nucleus. The existence of a hyperfine structure anomaly alters Eqs. (2) and (3) to the extent that H_n may no longer be cancelled out as a constant factor from both the numerator and denominator of the left side of Eq. (2). A series of experiments to compare $g_0\mu_N H_n/g_1\mu_N H_n$ for a diamagnet in a large applied magnetic field with the same quantity for a ferromagnet gave no hyperfine structure anomaly within our experimental limit of error.[20] These were differential experiments which could have detected effects equivalent to 0.5 kG in the observed hyperfine fields. Thus we are safe in excluding hyperfine structure anomaly effects.

Since we wish to measure H_n with the greatest possible precision, we note two advantages in using the identical source and absorber technique: First there is the minor advantage of slightly increased sensitivity, which we define as proportional to $dv_1/dH=0.0323$ (mm/sec)/kG for the single-line source split absorber, and $dv/dH=0.0374$ (mm/sec)/kG for the identical

[19] H. H. Stroke, R. T. Blin-Stoyle, and V. Jaccarino, Phys. Rev. 123, 1326 (1961).

[20] L. Grodzins and N. A. Blum, Rev. Mod. Phys. 36, 470 (1964); L. Grodzins, N. A. Blum, and R. B. Frankel (to be published).

source-absorber arrangement. Secondly, there is the considerable advantage of greatly increased counting rate for a given source strength. The requirement of keeping the single-line source near zero field in the vicinity of a 130-kG water-cooled solenoid necessitates either a massive magnetic shield or a suitable buckout magnet at the source. In either case the main solenoid structure dictates that the source must be at least 12 in. from the center of the main solenoid. The identical source/absorber arrangement places them about 1 in. apart, symmetrically located with respect to the center of the solenoid. The difference between these two geometric configurations amounts to about an order-of-magnitude difference in the counting rates. The source strengths available, the basic geometry of the apparatus which had to fit into the high-field solenoid together with certain minimum requirements on the number of counts needed in order to obtain the required precision, and the allotted maximum solenoid running time, indicated that the only feasible approach was the identical source/absorber technique.

The experiment was performed using a 10-mCi ^{57}Co in metallic iron source and an ^{57}Fe-enriched metallic-iron foil absorber,[21] both at 4.2°K and both in an external longitudinal magnetic field of up to 135 kG. One of the three-line hyperfine spectra obtained is shown in Fig. 2. The calibration and linearity of the spectrometer were checked by measuring the magnetic hyperfine splitting in an iron foil absorber using a single-line source (^{57}Co in Cu) with both the source and absorber mounted at the top end of the velocity transducer in the direction away from the high-field solenoid. The calibration was performed with the high-field solenoid energized and with all electronic and mechanical systems operating just as they would if the source and absorber were in the high magnetic field. The fringing field at the source/absorber location was a few hundred gauss, which produced a negligible effect on the hyperfine spectrum. The calibration of the spectrometer was observed to change by about 1% as the current in the solenoid went from zero to its highest value; this change was due to the interaction of the external field with the pickup coil magnet, as the calibration constant [(mm/sec)/channel] is proportional to the field in the gap of the pickup coil magnet. The counting equipment included a xenon-filled proportional detector because of its good resolution for 14-keV γ rays and because of its insensitivity to the stray magnetic field, together with a conventional nuclear-pulse amplifier, a single-channel analyzer to select the 14-keV γ ray, and a multichannel analyzer to store transmitted γ-ray counts as a function of source velocity. The velocity drive was an electromechanical constant-acceleration system. The velocity pickup system, suitably amplified and biased, was used to drive

[21] The source and absorber foils were 0.375 in. in diameter ×0.001 in. thick and 0.625 in. in diameter ×0.0002 in. thick, respectively.

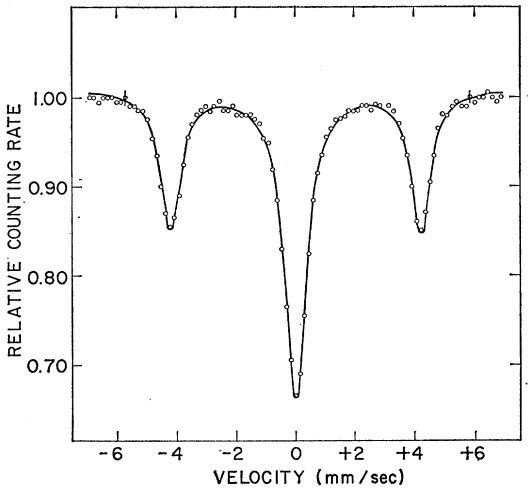

FIG. 2. Experimental absorption spectrum for ^{57}Co in iron foil versus ^{57}Fe in iron foil; both source and absorber are in a 133-kG external field. The solid line is a least-squares fit to the experimental data.

the address of the mutlichannel analyzer. Simultaneously, for normalization purposes, a second single-channel analyzer, selecting γ rays above the 14-keV window, was used to provide a counting rate unrelated to the source velocity; these pulses were stored in another segment of the analyzer memory. The field at the source and absorber locations was measured using a precision integrating fluxmeter, the accuracy of which was checked by comparison with a proton resonance in an NMR iron-core magnet.

The observed magnitude of the hyperfine field is given by

$$H_n = H_{\text{int}} + H_{\text{DM}} + \Delta H_1 - H_0, \qquad (4)$$

where H_{int} is the hyperfine field at zero external field (338 kG at 4.2°K), H_0 is the applied field, H_{DM} is the demagnetizing field[22] (21.8 kG for a thin iron foil), and ΔH_1 is the induced field at the nucleus which is taken to be proportional to the change in the magnetization. In Table I are listed the results of three separate determinations of ΔH for three values of H_0 above 100 kG. Combining these results, we obtain $\Delta H = 0.2 \pm 1.2$ kG.

TABLE I. Experimental results (in kG) from Mössbauer spectra for Fe versus Fe; $\Delta H_1 = H_{\text{int}} + H_{\text{DM}} - H_0 - H_n$.

H_0	H_n	$H_{\text{int}} + H_{\text{DM}}$	ΔH_1
133.4(5)	227.0(5)	360.0(5)	−0.4+1.2
133.0(5)	227.0(5)	360.0(5)	0 ±1.2
101.0(5)	259.2(5)	360.0(5)	−0.2±1.2

[22] Although the saturation value of H_{DM} is 21.8 kG, because of the anisotropy energy associated with the rotation of domains and movement of domain boundaries, we have experimentally determined that fields of the order of 30 kG applied perpendicular to the plane of the iron foil are necessary to align completely the magnetization along the external field direction.

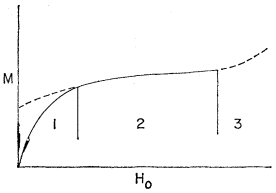

FIG. 3. General features of magnetization versus field. In region (1) numerous effects of impurities, strains, anisotropic contributions, domains, geometrical effects, etc., prevent saturation. In region (2) anisotropic contributions and spin-wave excitations still may play a role (in addition to band contributions to χ_{HF}). In region (3), the ultrahigh-field region, magnetic phase transitions may occur.

The hyperfine field measurement is related to the volume susceptibility,

$$\chi=\Delta M/\Delta H_0=(\Delta H_1/H_n)(M/\Delta H_0),$$

where ΔH_0 is the change in the external applied field, From this, we may write

$$\chi=[\Delta H_1 M]/[H_n(H_0-H_{\rm DM})], \qquad (5)$$

where M is the saturation magnetization in iron metal ($\sim$1.7 kG); thus $\chi\simeq(1\pm7)\times10^{-5}$ emu/cc. This result agrees with that obtained from the high-field magnetic moment measurement discussed here, but the possible error is somewhat larger; as can be seen from Table I, the error arises from the combined uncertainty in the applied field, the fitting of the data points and the spectrometer calibration.

C. Determination of Nuclear g Factors

These data may be used alternatively to determine the nuclear g factors independently of the electron-nuclear double resonance experiments.[23,24] To do this, we infer from the high-field susceptibility measurements described later in this paper that the term $\Delta H_1\cong0$; this is the same assumption made previously concerning the proportionality between M and $H_{\rm int}$. Since the splitting between the outer lines in the three-line spectrum is

$$v=2(g_1+g_0)\mu_N H_n(c/E_0), \qquad (6)$$

we find that

$$dv/dH_0=-2(g_1+g_0)\mu_N(c/E_0)[1-dH_{\rm DM}/dH_0]. \qquad (7)$$

For fields above 30 kG, $H_{\rm DM}$ is saturated and $dH_{\rm DM}/dH_0=0$. Using the best linear fit to the data above $H_0=30$ kG, we obtain $\Delta v/\Delta H_0=-3.69\times10^{-5}$ mm/sec/kG$\pm$1%. Thus $g_1+g_0=0.281\pm0.003$. From the usual six-line hyperfine spectrum (using an unsplit source) $g_0/g_1=1.750\pm0.004$;[17] we compute $g_0=0.179\pm0.002$ corresponding to a value for the ground-state moment $\mu_0=I_0g_0=(0.0894\pm0.001)\mu_N$ which agrees with the value $\mu_0=0.0903\pm0.0007\mu_N$ obtained by Ludwig and Woodbury[23] as well as with the most recent measurements of Locher and Geschwind[24] who obtained $\mu_0=0.09024\pm0.00007\mu_N$. This shows that the Mössbauer experiment may be viewed as a simple and direct method of measuring g_0, g_1, and H_n independently of the ENDOR experiments. The results using the two different techniques are essentially identical, as expected for a hyperfine anomaly which is less than our experimental error.

The high-field Mössbauer experiments on metallic iron may thus be considered in either of two ways: (1) As a confirmation of the susceptibility experiments giving a value for $\chi\simeq(1\pm7)\times10^{-5}$ emu/cc. (2) As a measurement of the ground-state nuclear magnetic moment of ^{57}Fe independent of the ENDOR experiments giving a value for $\mu_0=(0.0894\pm0.001)\mu_N$. Combining the Mössbauer and ENDOR results we conclude that the value of μ_0 is field-independent to 0.1% up to 150 kG.

III. MAGNETIC-MOMENT MEASUREMENTS

A. General Remarks

Before discussing the static magnetic-moment measurements we briefly consider the orders of magnitude involved. While high-field susceptibilities here are as small as $\chi_{\rm HF}\simeq1\times10^{-5}$ emu/cc ($\sim10^{-6}$ emu/gm) they can be measured readily by many techniques. However, when such values of χ are superimposed on a large background magnetic moment, a number of usually negligible factors must be considered. To measure $\chi_{\rm HF}=\Delta M/\Delta H_0$ to 10% we have $\Delta M=\chi_{\rm HF}\Delta H_0/10=0.1$ emu/cc for $\Delta H_0=10^5$ G. Since $M_s\simeq500$ G for Ni, we require that the background contributions to M_s vary by less than 2×10^{-4} for the entire field range. Thus, it is apparent that high sensitivity is not crucial here, but very high *differential* sensitivity and reproducibility is. Furthermore various anisotropic effects must be eliminated to high order, and *high fields are essential for measurements well beyond technical saturation.* More stringent conditions must be met when ΔH_0 is reduced. Finally, we note that we are attempting measurements of $\Delta M\simeq0.1$ G in the presence of field changes of $\Delta H_0\simeq10^5$ G which requires careful elimination of any background field effects of the applied magnetic field. For flux integration measurement techniques, the background ΔH_0 must be suppressed by a factor of more than 10^6.

B. Approach to Magnetic Saturation

The approach to magnetic saturation as a function of field is illustrated in Fig. 3. In the low-field region (1) numerous contributions including strains, impurities and anisotropic effects limit complete saturation. Region (2) involves high fields where most of these limiting interactions are overcome; but anisotropic and spin-wave contributions may still be present. By employing unstrained single-crystal samples and carefully

[23] G. W. Ludwig and H. H. Woodbury, Phys. Rev. **117**, 1286 (1960).
[24] P. R. Locher and S. Geshwind, Phys. Rev. **139**, A991 (1965).

applying the high-field along principal magnetic-symmetry axes, the anisotropic effects can be reduced to a negligible value in some cases. The spin-wave contribution can be suppressed by reducing the temperature. Region (3) is reversed for ultra-high fields where the interaction between the applied field and the magnetic system may be large enough to produce magnetic phase transitions.

Before the high-field susceptibility χ_{HF} can be evaluated, one other effect must be eliminated—that is, depolarizing (geometry) effects of the sample. Ideally, ellipsoidal samples should be used in order to assure that M is uniform in the sample. A general discussion of the depolarizing effects on a right-circular cylinder is discussed in Appendix A. The effects for Fe and Ni are not small unless fields well above 50 kG are employed.

C. Experimental Arrangement for High-Field Differential Susceptibility Measurements

Preliminary experiments were performed in an 80-kG superconducting magnet with a standard vibrating-sample magnetometer[25] (VSM) with a small spherical ferromagnetic single crystal at 4.2°K. Axial pickup coils were rigidly clamped to the superconducting magnet bore to assure minimum-vibration background. Sensitivity, which was 10–100 times greater than the usual transverse arrangement,[25] was certainly not a problem, but reproducibility and sample positioning required great care. The measurements showed that $\Delta M/M_s$ was less than 1% up to 80 kG. As discussed above, the limited range of applied fields available with a superconducting magnet was a serious problem. A new method of measurement was therefore devised which employed the high-powered water-cooled solenoids at the Francis Bitter National Magnet Laboratory. This method is briefly described below and was employed for the measurements discussed in this paper. Details of this instrument are discussed elsewhere.[26]

The method used for these high-field magnetic-moment measurements is a modification of the sample-extraction technique. The sample was moved between two series-opposing coils in a cyclic manner. The magnetizing field was supplied by dc solenoids ($2\frac{1}{8}$-in. inside diameter) with fields to 150 kG. The stability of the dc magnets is about 0.02% rms which leads to relatively large background field fluctuations. These are minimized by careful balancing of the pickup coils to 0.1%, careful positioning of the coil-pair in the dc solenoid in order to further minimize the background pickup, and finally by additional adjustment of the relative balance by a resistive dividing network placed across the two coils. Further reduction was effected by integrating the field fluctuations, additional electronic filtering, and finally by recording and time-averaging techniques.

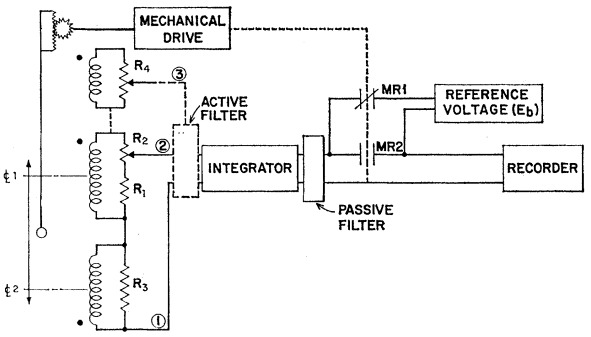

FIG. 4. Block diagram of the very-low-frequency vibrating-sample magnetometer (VLFVSM). The rack and pinion drive (upper left) moves the sample (sphere) *past* the effective centers of the series opposing pickup coils. The mechanical drive is coupled synchronously to mercury relays MR1 and MR2 which permit the stabilized reference voltage E_b to be inserted in series with the integrated output signal before recording. In this way high differential sensitivity is attained. Resistors R_1, R_2, and R_3 permit fine balancing of the pickup coils. Optional filtering and fine balancing is furnished by the components with dashed lines.

A significant and essential feature of this measurement method is the specific sample motion adopted. In order to assure reproducible sample positioning and repositioning under the influence of the large forces present in the high fields, the sample was moved *beyond* the effective centers of the coils. In this way it was not necessary to reproduce the exact sample position. Since the integrated output was recorded for each sample oscillation, the effective center was then readily determined from the recorded data. A second feature essential for accurate differential measurements was a method for subtracting at least 99% of the signal in a highly accurate manner so that the small differential field-dependent change in M could be displayed on an expanded scale. The schematic arrangement of the magnetometer and the differential balance circuit is shown in Fig. 4. A stable reference signal subtracted an accurately prescribed voltage from the integrated output synchronous with the sample drive. Only the extremes of the sample excursion were recorded as a function of time. An example of the differential output display is shown in Fig. 5. It should be mentioned that the sample moved only a few thousandths of an inch beyond effective coil centers for this display.

In order to time-average the field fluctuations as well as to permit recording of the output, a very low frequency drive (0.1–0.5 Hz) was furnished by a motor drive and cam arrangement. Integration of each cycle was accomplished with a low-drift operational amplifier system. Whenever possible, mechanical and electronic tolerances were carefully examined in order to minimize sources of error.

[25] S. Foner, Rev. Sci. Instr. **30**, 548 (1959).

[26] S. Foner and E. J. McNiff, Jr., Rev. Sci. Instr. **39**, 171 (1967). This method is specifically designed to compete with a high noise background and has a much lower sensitivity compared to the conventional VSM (Ref. 25). It does allow magnetic moment measurements in high fields with large field gradients, on strongly ferromagnetic samples.

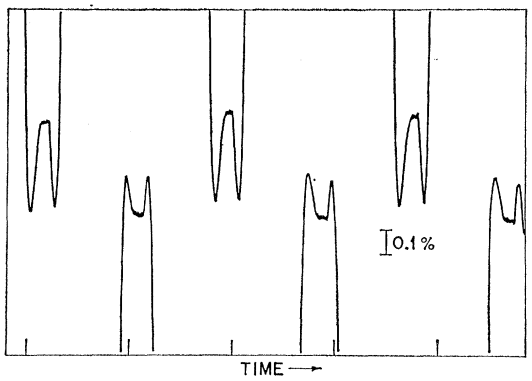

FIG. 5. Trace of differential magnetic moment (vertical scale) for fixed field versus time shown on an expanded scale. A change of 0.1% is indicated for comparison with noise and drift. The peaks correspond to the effective coil centers which are passed twice for each coil during the cycle. Data are obtained by time-averaging a series of the peaks and comparing the displacement between the upper and lower peaks as a function of field.

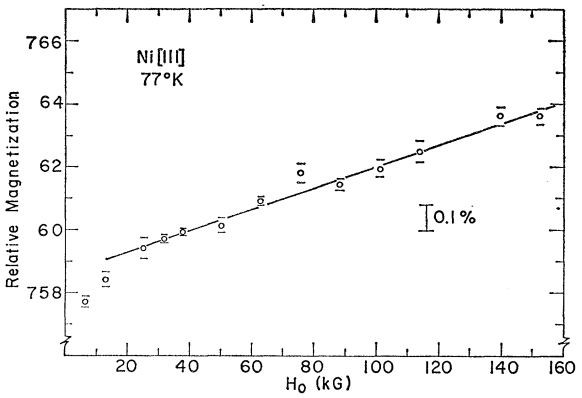

FIG. 7. Relative magnetic moment versus applied field H_0 for single-crystal Ni at 77°K. H_0 is parallel to ⟨111⟩.

Differential magnetic-moment measurements were taken at fixed fields and at fixed temperatures furnished by liquid He or N_2 and at room temperature. The average magnetic moment was determined by examining the time average of 10–20 oscillations. In this way systematic drifts were minimized. Various schemes were employed to minimize any systematic errors. For instance, data were taken in a sequence starting with low-field to high-field points, or by randomizing the field points in attempts to find any systematic time drifts of the data.

Many tests for systematic errors were made. A minimum clearance between the sample support rod and pickup coil mount was employed so that the sample was restricted from any radial motion (cf. Appendix B). All elements were rigidly clamped in the glass Dewar system to avoid motion of the coils in the applied field. Blank supporting mounts were measured versus field before and after a given magnetic-moment-measurement series to assure that any coil motion in the applied field produced a negligible signal. A substitute brass sample was tested at low temperatures in order to generate an eddy-current background effect comparable to that of the magnetic sample. Accurate magnetoresistance measurements of the pickup coils were made in order to correct for this contribution to the integrator calibration. Although a series resistance of at least 100 kΩ was used in the integrator input circuit, a magnetoresistive correction (linear above 30 kG) of as much as 0.1% was required over the complete range of field. This magnetoresistance correction was negligible at 77 and 300°K. A very useful systematic check was examination of the field dependence of M versus H over a wide range field. Whenever an appreciable nonlinear variation of M versus H_0 was detected, it was found that the coils were not sufficiently rigidly supported.

The samples were machined single-crystal Fe and Ni spheres, nonpreferentially etched in order to remove the strained surface. In one case an approximately prolate ellipsoidal Fe crystal sample was cut in order to examine the field dependence when the major axis was parallel or perpendicular to the field. In this way effects of possible torques on the sample resulting in radial sample position changes or induced coil motion

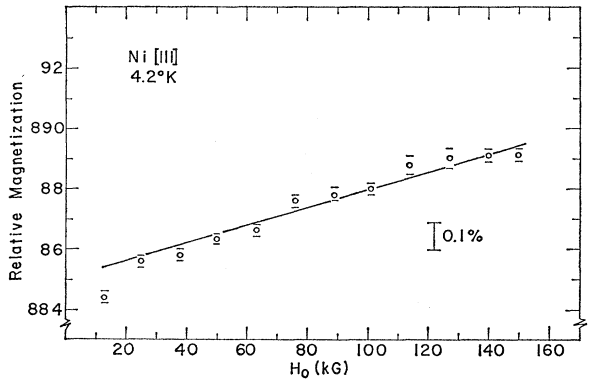

FIG. 6. Relative magnetic moment versus applied field H_0 for single-crystal Ni at 4.2°K. H_0 is parallel to ⟨111⟩.

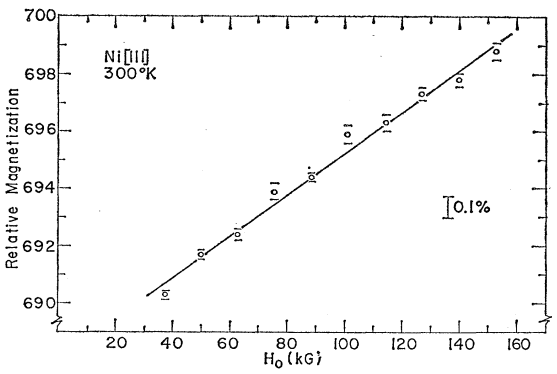

FIG. 8. Relative magnetic moment versus applied field H_0 for single-crystal Ni at 300°K. H_0 is parallel to ⟨111⟩.

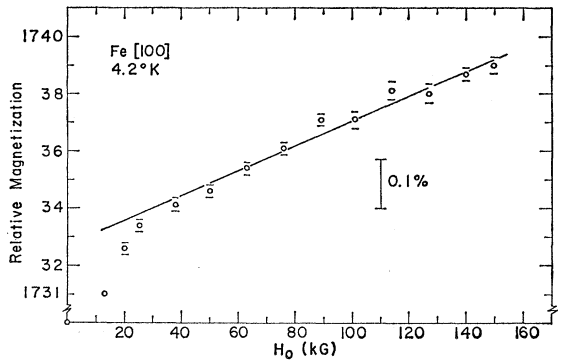

FIG. 9. Relative magnetic moment versus applied field H_0 for single-crystal Fe at 4.2°K. H_0 is parallel to ⟨100⟩.

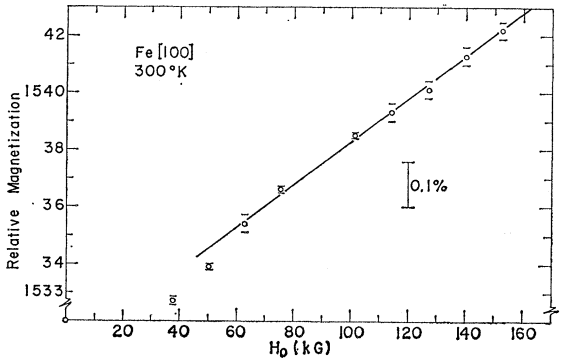

FIG. 11. Relative magnetic moment versus applied field H_0 for single-crystal Fe at 300°K. H_0 is parallel to ⟨100⟩.

were examined. These torques would produce a nonlinear M versus H variation and a noticeable difference in the high-field susceptibility. Such effects were not detected.

D. Experimental Results

The differential magnetic moment for Ni and Fe single crystals as a function of H_0 along the easy axes are shown in Figs. 6–11. The straight lines are obtained by least-square fitting of the data points where each is given equal weight. Only the *relative magnetization* is displayed on the vertical axis since we are examining the differential moment. Note that the absolute magnetic moment may not be deduced from the scale because corrections for the temperature dependence of the pickup-coil resistance and the other factors have not been made. In fact, no absolute measurements of magnetic moment need be made for our purposes here, only the relative changes at fixed temperature are required. The known magnetic moment for these metals is used as a self-calibration. The data points correspond to averages over a large number of oscillations at fixed field. Each datum point is corrected for both the measured nonlinear magnetoresistance of the detection coils (see, e.g., Fig. 9, Ref. 26) and background noise. The largest magnetoresistive correction was about 0.1% for the relative magnetic moment at highest field. This magnetoresistance is measured directly to at least 0.1% so that any systematic error here is negligible. We also note that this correction is negligible for the Ni data at 77 and 300°K and for Fe at all temperatures. The noise correction is small (about one error bar in the most extreme case) and involves a certain value judgment of the peak-to-peak average noise measured at the beginning or the end of each datum-point observation.[27] There is a general tendency for an approximately linear increase of the peak-to-peak noise with H_0 since many of the noise sources scale with H_0. Occasionally interference from other sources (other experiments sharing the generator output) produced slightly larger noise during a particular run and this peak-to-peak noise correction was made. The error bars shown in Figs. 6–11 indicate only the *peak-to-peak* variation of the time-averaged differential magnetic moment data for the spherical single-crystal Ni and Fe samples.

Nonlinearities in the χ_{HF} data were examined in various ways in order to detect systematic or real

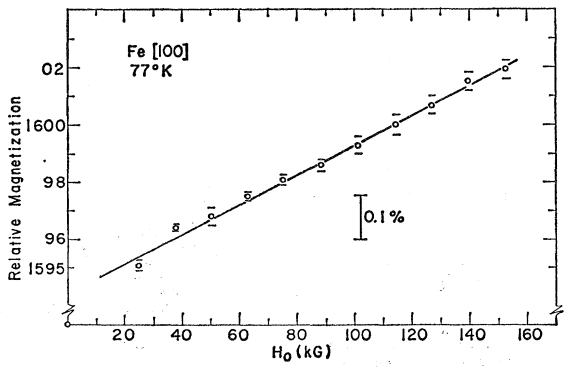

FIG. 10. Relative magnetic moment versus applied field H_0 for single-crystal Fe at 77°K. H_0 is parallel to ⟨100⟩.

TABLE II. Tabulation of linear fit from 50–150 kG for high-field susceptibility χ_{HF} for Fe and Ni.[a]

	4.2°K	77°K	300°K
Ni[111]	1.69(0.11)	2.27(0.20)	5.21(0.18)
Fe[100]	4.31(0.12)	5.48(0.29)	9.10(0.42)

[a] Units of χ_{HF} in 10^{-5} emu/cm³. (Standard errors are shown in parentheses for each value of χ_{HF}.)

[27] It should be mentioned that these noise corrections were applied to all the data in Figs. 6–11 because the cyclic sample motion was rapid for these runs so that the peak-to-peak noise was superimposed on the recorded trace. For much lower-frequency cyclic motion, a noise correction is not required because the noise is clearly averaged for each oscillation. Such a case is shown in Fig. 5 where the noise produces a slightly thicker trace. The data under such conditions agree well within our quoted experimental errors for the faster cyclic data. However, the later data are slightly more accurate because the major systematic error does not arise from the noise correction, but instead from integrator and field drift during the much longer running time required for each sequence of data points.

TABLE III. Variation of χ_{HF} with range of applied field ΔH_0.[a]

	Ni			Fe		
ΔH_0(kG)	4.2°K	77°K	300°K	4.2°K	77°K	300°K
101–150	1.22(0.18)		4.18(0.25)	3.57(0.71)		8.31(0.68)
89–150	1.33(0.15)	2.49(0.23)	4.88(0.31)			
76–150	1.32(0.11)	2.12(0.36)	4.82(0.20)	3.68(0.36)	5.62(0.27)	8.36(0.46)
63–150	1.59(0.11)	2.10(0.23)	5.17(0.22)	4.01(0.23)		8.52(0.40)
50–150	1.69(0.11)	2.27(0.20)	5.21(0.18)	4.31(0.12)	5.48(0.29)	9.10(0.42)
38–150	1.75(0.08)	2.26(0.15)	5.40(0.15)	4.45(0.15)	5.33(0.09)	9.15(0.38)
25–150	1.77(0.09)	2.27(0.13)				

[a] Units of χ_{HF} in 10^{-5} emu/cm^3. (Standard errors are shown in parentheses for each range.)

deviations. One procedure was to least-squares fit the data for the same data points by successively removing the lowest-field point only; then in the next fit to remove the lowest two points; then the lowest three, etc. Generally, we find that there is a slight curvature of the data so that the highest-field data lead to a slightly smaller χ_{HF} than the linear average over a large range of field. At present it is not clear whether this curvature involves a systematic error in the experiment or a real effect. Again it should be noted that the apparently field-dependent χ is most noticeable for χ_{HF} of Ni at 4.2°K. If we use all the high-field data points above technical saturation, the χ_{HF} for an assumed linear variation of M versus H_0 is given in Table II for Ni and Fe. The effect of removing successive low-field data points for Ni and Fe is shown in Table III. Finally, a quadratic variation of M versus H_0 was examined, although this effect (Appendix A) is not expected for our spherical sample geometry. The results of the quadratic least-squares computer fit lead to smaller values of χ_{HF} than those in Table III.

To summarize, we find that the largest values of χ_{HF} are obtained by assuming a linear variation of M versus H_0. This is the result which would be obtained by examining just the end points at low and high fields above technical saturation. All the procedures which remove low-field data systematically lead to smaller values of χ_{HF}; the largest percentage reduction being observed for the smallest χ_{HF} (i.e., for Ni at 4.2°K). Thus the linear fit leads to the largest possible χ_{HF}. These results should be borne in mind in the discussion of the results.

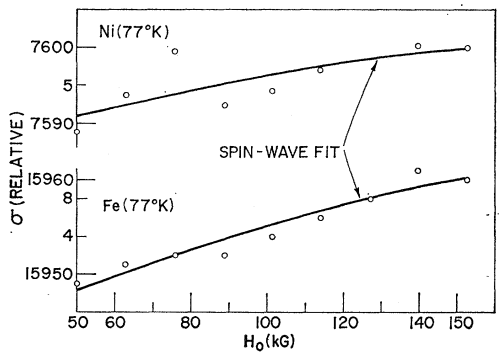

FIG. 12. Spin-wave fit (solid lines) to relative magnetic moment versus field H_0 for Fe and Ni single-crystal data at 77°K. The relative scale is ten times that of Fig. 7.

E. Spin-Wave Contributions at High Temperatures

Spin-wave contributions to χ, which are small at low temperatures (because few spin waves are excited) become appreciable at higher temperatures because the applied magnetic field diminishes the magnon contribution to the magnetization arising from the thermal excitation of spin waves. This may be seen from the temperature and field dependence of the magnetization[3]

$$M(H,T)\approx M_0\{1-a_{3/2}[F(\tfrac{3}{2},t_H)/\zeta(\tfrac{3}{2})]T^{3/2} -a_{5/2}[F(\tfrac{5}{2},t_H)/\zeta(\tfrac{5}{2})]T^{5/2}\}, \quad (8)$$

from which $\chi=\partial M/\partial H_0$ may be obtained. The functionals $F_n(t_H)$, defined as

$$F_n(t_H)=\frac{1}{\Gamma(n)}\int_0^\infty \frac{x^{n-1}dx}{\exp(t_H+x)-1}=\sum_{p=1}^{\infty} p^{-n}e^{-pt_H} \quad (9)$$

with $t_H=g\mu_B H_0/kT$, give the magnetic-field dependence of the reduced spin-wave terms. In Appendix C we have tabulated $F_{3/2}(t_H)$ and $F_{5/2}(t_H)$ for various temperatures and a wide range of fields. Derivatives with respect to temperature and field are also tabulated because they are becoming increasingly useful particularly where high-sensitivity ac modulation techniques are applied to ferromagnetic systems.

The temperature dependence of M versus H_0 for spin waves is included in Eq. (8) for Ni and Fe. Thus one may use χ_{HF}(4.2°K) as a reference value which is subtracted from the higher temperature χ_{HF} in order to estimate the spin-wave contributions at these temperatures. The results give $a_{3/2}=(8.8\pm2.9)\times10^{-6}$ for Ni when $\chi_{HF}(4.2°K)=1.7\times10^{-5}$ and $a_{3/2}=(5.7\pm1.7)\times10^{-6}$ for Fe when $\chi_{HF}(4.2°K)=4.3\times10^{-5}$. The errors in $a_{3/2}$ preclude evaluation of $a_{5/2}$. From the data of Argyle *et al.*[2] we have values of $a_{3/2}=(7.5\pm0.2)\times10^{-6}$, $a_{5/2}=(1.5\pm0.2)\times10^{-8}$ for Ni, and $a_{3/2}=(3.4\pm0.2)\times10^{-6}$, $a_{5/2}=(1\pm1)\times10^{-8}$ for Fe. At 4.2°K and for

fields above 50 kG these contributions to χ_{HF} at 4.2°K are negligible (see Appendix C). The spin-wave contributions deduced here are seen to be in good agreement with the more accurate values obtained earlier by measurements of M versus T. A plot of the computer fit (solid line) is compared with experiment for Ni and Fe at 77°K with the above values of $a_{3/2}$ in Fig. 12. Although our values of $a_{3/2}$ are reasonable, measurement of the temperature dependence of χ_{HF} is a rather difficult and indirect method of evaluating spin-wave contributions. Also to be considered is the apparent H_0 dependence of χ_{HF} shown in Table III; we have used the average value of χ_{HF} from 50–150 kG for our discussion in the text.

F. Discussion of Related High-Field Susceptibility Data

An upper limit to χ_{HF} in Fe and Ni at (288°K) temperatures was obtained by Kapitza[28] with pulsed fields of 250 kG. He found that ΔM was less than $\pm 1\%$ (his experimental error) over the field range employed. Until recently this upper bound was the best available. For Ni and Fe, χ_{HF} was found to be 0 ± 2 and $0\pm 8\times 10^{-5}$ emu/cm^3, respectively.[29] These limits are lower than our measured values at 300°K.

Recently, two groups of researchers reported independent measurements of χ_{HF} in ferromagnets,[6,7] Measurements of Herring *et al.*[7] (HBCM) presented for Fe and Ni to 50 kG gave χ_{HF} of 11 and 5×10^{-5} emu/cm^3 respectively. These results were obtained with fields generated by a superconducting magnet (and are stated to be more precise than their higher-field data in water-cooled solenoids).[7] At the same time Freeman *et al.*[6] reported the results of the Mössbauer and high-field magnetic measurements which gave $\chi_{HF}<4\times 10^{-5}$ and 1.1×10^{-5} emu/cm^3 for Fe and Ni, respectively.

Shortly thereafter Stoelinga and Gersdorf[8] presented results with several tenths of a second pulsed fields to 200 kG for Fe and Fe-Co alloys and for Ni. Their values of χ_{HF} for Fe and Ni at 4.2°K are 3.3×10^{-5} and 2.0×10^{-5} emu/cm^3 and are in approximate agreement with our data. The latter results are remarkable since, for pulsed fields, there are a number of possible systematic errors which are difficult to examine in a direct way. As in Kapitza's results, these pulsed-field data are aided by the large range of field available for their measurement.

Because the χ_{HF} data of HCBM are considerably larger than our results and yet employ dc fields we will briefly discuss some basic differences. Our own detailed investigations using both superconducting and water-cooled magnets have suggested possible physical causes for these differences. First, HBCM data involves relatively low magnetizing fields. This requires much higher accuracy in measurements as well as an extremely more refined control of systematic errors. In addition, the limited field range makes it quite difficult to observe small but significant sources of error. Second, the superconducting solenoid adds some additional problems which are not readily eliminated. These include (a) the shielding effects of the superconducting wire which are H_0-dependent and thus affect the coupling between the sample and detection coil; (b) the effects of the solenoid current stabilizing supply on the pickup voltage which can be very large if the solenoid is voltage stabilized rather than current stabilized and, if the detection coils are closely coupled to the magnet. The moving sample can induce a small voltage in the multiturn superconducting solenoid which in this case is detected and compensated for by the current supply (when operating in the constant voltage mode), but in the process of compensation the flux in the pickup coils is changed slightly; (c) a closely related effect occurs if the superconducting magnet is stabilized with a superconducting shorting link. In this case the flux linked to the magnet remains constant as the sample is moved and the flux change at the detection coils is partially compensated; (d) the sample position is more critical particularly for the smaller range of field used for the measurement; (e) if the sample is not ellipsoidal, small depolarizing effects are extremely important in the lower field range (see Appendix A); (f) unless exceptionally high-field homogeneity of the superconducting magnet and exceptional balance of detection coils are achieved, small changes in the field distribution can be sensed as effective changes in the distribution of the sample magnetization so that again a source of error arises. In addition, the field drift must be negligible. Again we emphasize that although these effects are often of second or higher order in the usual experiments. here such effects can yield significant systematic errors of the differential susceptibility. We have made a number of tests with our techniques in superconducting solenoids and readily detected some of these effects.

We have attempted to reexamine the data of HBCM for Ni at 4.2°K employing terms both linear and quadratic in H_0. A least-square fit of their data from 15.5–50 kG yield $\chi=3.8\times 10^{-5}$ emu/cm^3 (with a sizable curvature) and for 22.8–50 kG, $\chi=4.9\times 10^{-5}$ emu/cm^3 (also with an appreciable curvature). The results at present are rather large compared to all other higher-field data. However, the general feature of a nonlinear M versus H_0 and a large curvature suggests incomplete saturation. Examination of our data in Table III also shows evidence of a somewhat higher χ at low fields. The above conclusion is also consistent with the HBCM Fe data. One expects that systematic errors arising from sources other than the sample would be relatively smaller for Fe than for Ni. However, as observed, incomplete saturation would be even more of a problem in the low-field region since M_s is much larger for Fe.

[28] P. Kapitza, Proc. Roy. Soc. (London) **A131**, 243 (1931).

[29] W. Henry, Phys. Rev. **99**, A668 (1955) reports an upperlimit χ_{HF} of about $\pm 9\times 10^{-5}$ emu/cc for Fe at 4.2°K and below.

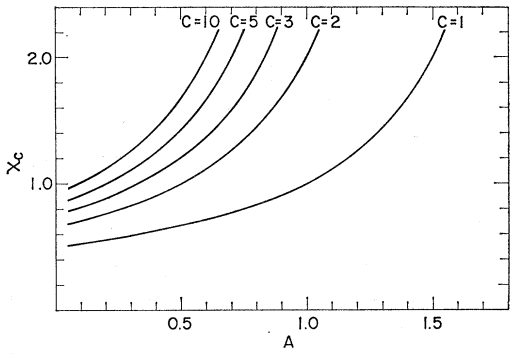

FIG. 13. Parametric plot of χ_c (calculated χ_{HF}) for two-band model for characteristic ratios of density of states for up- and down-spin bands versus band-splitting energy [see Eq. (10)].

In all respects it appears that many incidental effects can be most effectively eliminated by extending measurements to the 100–200 kG range for studies of χ_{HF} in ferromagnets.

IV. INTERPRETATION OF RESULTS

To interpret the results and thus obtain information about the band structure of the ferromagnetic metals Fe and Ni, we now examine various contributions to χ_{HF}. We will not include many-body contributions both because their significance is not known in detail,[1] and because this would further greatly complicate our qualitative discussion. The magnetic susceptibility of a transition metal, based on a simplified tight-binding model of two types of partially filled bands (d and s) occupied up to the Fermi energy, includes the following contributions:

(i) The Pauli spin paramagnetic contribution from the s band χ_s.

(ii) The Pauli spin paramagnetic contribution from the d band, χ_d. As is well known, both (i) and (ii) are taken to be the result of a redistribution of the occupation of the spin-up and -down bands by the applied magnetic field.

(iii) The paramagnetic contribution, χ_{VV}, for partially filled degenerate bands, or the Van Vleck temperature-independent paramagnetism for metals.[30] This term arises from the mixing of excited states into the ground state by the additional magnetization term in the Hamiltonian. For metals this mixing, which is between the occupied Bloch states below the Fermi energy E_F and the empty Bloch states just above E_F, may become appreciable. Since *ab initio* calculations of χ_{VV} require detailed knowledge of the band structure few such calculations have been carried out.

(iv) The diamagnetic contributions χ_{dia} arising from the Larmor diamagnetism of the core electrons and the Landau conduction electron diamagnetism.

(v) Spin-wave contributions χ_{sw}. The amplitudes of the thermally excited spin waves are decreased by increasing H and/or decreasing T.

To deduce information about the band structure of ferromagnetic metals from measurements of χ at low temperatures, i.e., to obtain χ_d, we must first estimate the other contributions to χ. Where possible we use experimental data, rather than theoretical estimates, because the latter are somewhat less reliable at this time.

Estimates of χ_{dia} may be obtained from measurements of χ in Cu where the d band is completely full by subtracting a free electron estimate for the s-electron susceptibility. We obtain $\chi_{dia}=-1\times10^{-6}$ (units of χ are in emu/cc) which may be considered an upper limit because in both Fe and Ni the d bands are not both completely full and it is known that the $3d$ electrons make the major contribution to χ_{dia}. Similarly χ_s is very small in Ni (0.9×10^{-6} in the free electron approximation for 0.6 s electrons and 1×10^{-6} for one s electron).

A much larger contribution arises from χ_{VV} for which estimates have been made for a number of metals including paramagnetic Ni. In some cases Knight shift data have been used to determine χ_{VV} (although none of these considered ferromagnetically occupied bands).[31] Mori[32] has computed χ_{VV} to be 1.3×10^{-5} emu/cc using Fletcher's[33] tight-binding calculations for nonmagnetic Ni, whereas Shimizu *et al.*[34] find $\chi_{VV}=1.1\times10^{-5}$ and 0.6×10^{-5} (if a molecular field term is or is not included respectively). We should note that published values of χ_{VV} include Cr (Ref. 35) (2.0×10^{-5} (Ref. 36) and 2.2×10^{-5}), V (Ref. 37) (2.3×10^{-5}) Pt (Ref. 38) (0.3×10^{-5}). It is seen that these values show a crude proportionality to the product of the number of holes and electrons in the d bands and that the maximum χ_{VV} estimate is less than 2.5×10^{-5}. We shall assume in what follows, that $\chi_{VV}\simeq1.1\times10^{-5}$ for Ni and 1.5×10^{-5} for Fe. (An entirely independent estimate of χ_{VV} given in Ref. 7 yields an essentially identical result for Ni.) As we shall see, while this assumption is not important for the interpretation of the band occupancy in Fe, it is important for the case of Ni.

[30] R. Kubo and Y. Obata, J. Phys. Soc. (Japan) **11**, 547 (1956); see also recent work by C. M. Place and P. Rhodes, J. Appl. Phys. **39**, 1282 (1968).

[31] V. Jaccarino, in *Magnetism*, edited by G. T. Rado and H. Suhl (Academic Press Inc., New York, 1965), Vol. IIA, p. 307; A. Narath, in *Hyperfine Interactions*, edited by A. J. Freeman and R. B. Frankel (Academic Press Inc., New York, 1967).

[32] N. Mori, J. Phys. Soc. (Japan) **20**, 1383 (1965).

[33] G. C. Fletcher, Proc. Phys. Soc. (London) **A65**, 192 (1952).

[34] M. Shimizu, T. Takahashi, and A. Katsuki, J. Phys. Soc. (Japan) **18**, 801 (1963).

[35] M. Shimizu, T. Takahashi, and A. Katsuki, J. Phys. Soc. (Japan) **17**, 1740 (1962).

[36] M. Shimizu and A. Katsuki, J. Phys. Soc. (Japan) **19**, 614 (1964).

[37] A. M. Clogston, A. C. Gossard, V. Jaccarino, and Y. Yafet, Phys. Rev. Letters **9**, 262 (1962).

[38] A. M. Clogston, V. Jaccarino, and Y. Yafet, Phys. Rev. **134**, A650 (1964).

By contrast, we note that the spin-wave contribution to the change in magnetization with field is completely negligible ($\chi\sim10^{-8}$) at 4.2°K in the range of fields used here. At higher temperatures χ_{sw} is of course much larger.

Estimates of χ_d can be made from band calculations using Eq. (1), but these are of necessity crude because in ferromagnets both the density of states term and the exchange term have approximately the same value. Note that while we have separated out χ_s from χ_d in the above discussion the $N(\epsilon)$ terms from energy-band calculations contain combined s and d contributions; we shall use χ_d to denote the combined-band susceptibility. Since χ_s is very small, only a small error is made in using either procedure, but this definition does serve as a basis for making comparisons.

A number of energy-band calculations have been done for both Fe and Ni in the paramagnetic state. To see the sensitivity of χ_d to the calculated $N(\epsilon_F)$ values consider the following: For Fe, Wood[39] has estimated $N(\epsilon_{F\uparrow})=0.84$ and $N(\epsilon_{F\downarrow})=0.38$ states/spin eV atom using his nonmagnetic augmented plane-wave calculations and a *rigid-band* splitting of these energy bands chosen so as to reproduce the observed magnetic moment. Using his value of the band splitting $\Delta E(=2k\theta')=0.94$ eV gives a large χ_d (2×10^{-4}). On the other hand using similar density-of-states values, calculated by Cornwell and Wohlfarth[40] from Wood's energy bands [$N(\epsilon_{F\uparrow})=0.75$ and $N(\epsilon_{F\downarrow})=0.35$ states per spin per atom per eV] and their band-splitting energy (i.e., $2k\theta'=1.35$ eV), gives a negative χ_d from Eq. (1)—clearly a meaningless and non-self-consistent result. However, if we arbitrarily use $2k\theta'=1.4$ eV, as estimated by Wohlfarth[41] from an analysis of various

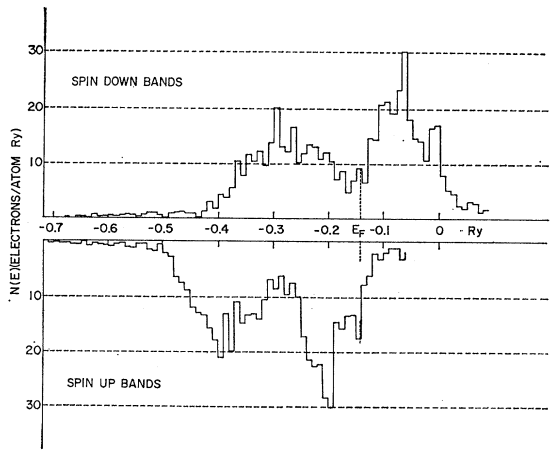

FIG. 14. Histogram of total density of states for spin-up and spin-down bands versus energy of Fe obtained by Wakoh and Yamashita (Ref. 9).

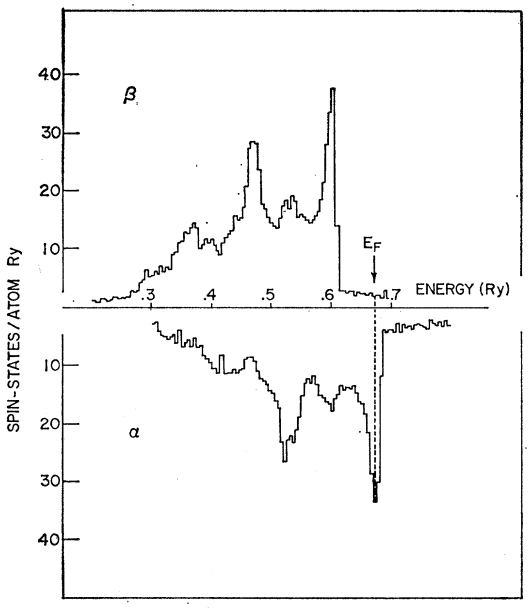

FIG. 15. Histogram of total density of states for spin-up and spin-down bands versus energy of Ni obtained by Connolly (Ref. 10).

data, and use Wood's $N(\epsilon)$ values (which are now unrelated) we obtain $\chi_d=1.7\times10^{-5}$ which is close to the experimental value (obtained by subtracting $\chi_{VV}=1.5\times10^{-5}$ from our measured χ_{HF}). Alternatively, if one accepts Wood's $N(\epsilon_F)$ values then a $k\theta'=0.6$ eV would reproduce the measured χ_d value for Fe taken as $(\chi-\chi_{VV})=2.5\times10^{-5}$. In any event, our results and these crude estimates point up some of the uncertainties in both the theoretical calculations and in our knowledge of the molecular field parameter.

The parameters examined above give only a very qualitative estimate of χ_d. In the spirit of our discussion we may assume Eq. (1) holds and treat $k\theta'$ as a parameter to be determined by experiment. Equation (1) can be rewritten as

$$\chi_c=\frac{C/(1+C)}{1-[C/(1+C)](4N_2k\theta')/n}, \tag{10}$$

where $N_1=CN_2$ ($N_1\geq N_2$), N_1 and N_2 are the densities of states of the two bands, and $\chi_c=\chi_d/4\mu^2N_2$. Normalized plots can then be generated (cf. Fig. 13) versus $(4N_2k\theta')/n=A$ for chosen characteristic values of C. Experimental values of χ_d (suitably corrected for χ_{VV}, etc.) and values of C obtained from band calculations may then be used to determine $k\theta'$ (from band calculations or experiment). Alternatively, the range of $k\theta'$ and C may be examined for various values χ_d. Various estimates of N_1 and N_2 for Fe and Ni (based on band

[39] J. H. Wood, Phys. Rev. **126**, 517 (1962).
[40] J. F. Cornwell and E. P. Wohlfarth, J. Phys. Soc. (Japan) **17**, Suppl. B1, 32 (1962).
[41] E. P. Wohlfarth [in *Proceedings of the Nottingham Conference on Magnetism* (The Institute of Physics and the Physical Society, London, 1964), p. 51] has an extensive summary of various estimates of $k\theta'$.

calculations[9–11]) yield values of $k\theta'$ well within the range expected.[41]

More appropriate for comparison with our experimental results are spin-polarized self-consistent band calculations for the ferromagnetic state obtained by the use of different potentials for different spin. Since our first report,[6] such calculations have been published for Fe by Wakoh and Yamashita[9] and for Ni by Connolly.[10] Their computed densities of states for spin-up and spin-down bands for Fe and Ni are shown in Figs. 14 and 15 plotted with a common ϵ_F in each case. The difference between these two ferromagnets is seen in a very striking fashion: whereas both spin bands in Fe are only partially filled and so a substantial band contribution to χ is expected, for Ni only one spin band has holes and so while $N(\epsilon_{F\downarrow})$ may be large, $N(\epsilon_{F\uparrow})$ is much smaller and hence a small band contribution to χ results. Since the exchange splitting of the bands is not a well-determined quantity in *ab initio* band calculations we will not attempt quantitative estimates of χ_d based on these results. Instead we compare our experimental value with recently published results of Hodges *et al.*[11] on Ni obtained by a (semiemperical) interpolation scheme.

Hodges *et al.*[11] have used their pseudopotential scheme to determine in a self-consistent way the band structure of ferromagnetic Ni. Correlation effects were incorporated through the use of an intra-atomic Coulomb interaction much like the one proposed by Gutzwiller,[42] Hubbard,[43] and Kanamori.[44] Good agreement was obtained with a number of experimental quantities. While their computed density of states curves for the spin-split bands resemble those obtained by Connolly,[10] the actual energy splitting (or separation) of the bands is much smaller and closer to that expected from other considerations.[41] Their computed $N(E_F)$ values, $N(\epsilon_{F\uparrow})=4.5$ states/Ry and $N(\epsilon_{F\downarrow})=22.6$ states/Ry, can be used to calculate a high-field band susceptibility χ_d at low temperatures if one replaces the collective electron formula, Eq. (1), by the expression

$$\mu_B^2/\chi_d=\tfrac{1}{4}[1/N(\epsilon_{F\uparrow})+1/N(\epsilon_{F\downarrow})]-\tfrac{1}{2}U_{\text{eff}}{}^{d-d}\textstyle\sum_\mu \tilde{n}_{\mu\uparrow}\tilde{n}_{\mu\downarrow} -\tfrac{1}{2}J_{\text{eff}}{}^{s-d}(\tilde{n}_{s\uparrow}-\tilde{n}_{s\uparrow}{}^2+\tilde{n}_{s\downarrow}-\tilde{n}_{s\downarrow}{}^2). \quad (11)$$

These last terms come from Gutzwiller-Hubbard-Kanamori form of the interaction Hamiltonian. In order to define the quantities $\tilde{n}_{\mu\sigma}$ and $\tilde{n}_{s\sigma}$, Hodges *et al.* note that in applying a large magnetic field to a ferromagnet, the populations of the orbitals $\mu\sigma$ will change by amounts $\delta n_{\mu\sigma}$. In terms of this change, $\tilde{n}_{\mu\sigma}=|\delta n_{\mu\sigma}/\delta n|$, where $\delta n=\delta n_{s\uparrow}+\Sigma_\mu \delta n_{\mu\uparrow}=-\delta n_{s\downarrow}-\Sigma_\mu \delta n_{\mu\downarrow}$. Similarly, $\tilde{n}_{s\sigma}=|\delta n_{s\sigma}/\delta n|$. On the basis of their calculations, Hodges *et al.* predicted a value for χ_d of 0.8×10^{-5} emu/cm^3 for Ni. This low value of χ_d which arises as we have seen from the very small value of $N(\epsilon_{F\uparrow})$, is in very good agreement with the χ_d value we determine from our experiments (the goodness depends on the size of χ_{VV}). In view of the various approximations to other contributions to χ, notably χ_{VV}, this good agreement may be accidental. Because this semiempirical calculation employs many of the experimental parameters it is difficult to assess to what extent the agreement is a necessary consequence.

[42] M. C. Gutzwiller, Phys. Rev. Letters **10**, 159 (1963); Phys. Rev. **134**, A923 (1964).
[43] J. Hubbard, Proc. Roy. Soc. (London) **A276**, 238 (1963); **A277**, 237 (1964); **A281**, 401 (1964).
[44] J. Kanamori, Progr. Theoret. Phys. (Kyoto) **30**, 275 (1963).

V. POSSIBLE SOURCES FOR FIELD-DEPENDENT HIGH-FIELD SUSCEPTIBILITY

In this section we examine sources of a field-dependent χ_{HF} at low temperatures. Such an effect is expected to be small and may be well below our present detection sensitivity. For this reason we examine this possibility only briefly.

A. Systematic Errors

In Sec. III systematic experimental errors were examined. Of the various possible sources we noted the following:

(1) The approach to saturation was limited by anisotropic effects and spin wave contributions—these were minimized by employing single crystal samples, magnetized along the easy axis at 4.2°K so that spin-wave contributions were completely suppressed at high fields (see Appendix C).

(2) Depolarizing effects of nonellipsoidal samples can produce a nonlinear χ_{HF} as described in Appendix A. However, spherical samples were employed in order to eliminate this effect.

(3) The search for any systematic field-dependent errors was extensive, but because the observed nonlinearity of $\chi_{HF}(H_0)$ borders on the level of the detection sensitivity of the moment measuring instrument, it is difficult to completely rule out a small systematic background effect.

Although the observed field dependence of χ_{HF} is of the order of our experimental uncertainty, in Sec. V B we consider properties intrinsic to the magnetic system which could lead to a field-dependent $\chi_{HF}(H_0)$.

B. Field-Dependent Susceptibility of Itinerant Ferromagnet

The Stoner model has been studied extensively[45] with various approximations but the change of the magnetic moment at $T=0$°K for laboratory accessible fields has been consistently dismissed for ferromagnetic metals

[45] A. H. Wilson, *The Theory of Metals* (Cambridge University Press, England, 1953), 2nd ed.

TABLE IV. Results of Stoner model calculations.

	$4\pi M_s$(kG)[a]	$N\uparrow$	$N\downarrow$	E_F(eV)[b]	$\chi(100\text{ kG})/\chi(H_0)[\chi(50\text{ kG})/\chi(H_0)]$ $H_0=150$ kG	$H_0=200$ kG	$H_0=250$ kG	$\epsilon\%$[c]
Fe	21.800	2.45	4.65	6	1.041[1.085]	1.081[1.130]	1.121[1.172]	0.173
				13	1.021[1.042]	1.041[1.162]	1.061[1.185]	0.044
Ni	0.105	0.295	0.305	7	1.310[2.08]	1.588[2.52]	1.844[2.92]	0.173
				14	1.308[2.07]	1.585[2.50]	1.838[2.90]	0.171
	0.206	0.29	0.31	7	1.304[2.04]	1.577[2.47]	1.827[2.86]	0.325
				14	1.298[2.02]	1.566[2.43]	1.812[2.81]	0.332

[a] The value of M_s for Ni is based on an assumed slight polarization of only the s bands.
[b] The densities of states at the Fermi energy E_F for up or down spin bands, $N\uparrow$ and $N\downarrow$, are given in states/spin Rydberg based on band calculations (Refs. 9 and 10).
[c] $\epsilon\%$ is the percent deviation of the magnetic moment from a straight line field dependence extrapolated from 50 kG.

with large spontaneous moments[46] on the grounds that the energy perturbing the system is much smaller than the Fermi energy. However, the sensitivity of the χ_{HF} measurements discussed in this paper and availability of very large magnetic fields require a reexamination of this effect.

We have, therefore, examined the variation of M with applied field for the Stoner model applied to Fe and Ni, with very simplified approximations. It should be emphasized that the purpose here was only to examine the *relative* change of χ_{HF} versus H_0 rather than the actual magnitude of χ_{HF}. These simplified calculations suggest that for a wide range of parameters the *relative* field dependence of χ_{HF} is model-independent. Although the values of χ_{HF} must involve realistic band calculations, we have applied the Stoner model for electrons in parabolic bands at $T=0°$K, and calculated M as a function of $H_0=50$, 100, 150, 200, and 250 kG. From these results we then determined the field-dependent χ_{HF}. The percent deviation ϵ of the actual moment from the straight line passing through the values at 50 and 100 kG was calculated for Fe and Ni. Representative values of ϵ are tabulated in Table IV. The calculations assumed that for Fe only the $3d$ bands contribute, while for Ni any $3d$-band contribution was neglected and only a fractional value of the spontaneous moment was assigned to the s band. Estimates of the densities of states were obtained from examination of recent band calculations.[9–11]

Although the calculations yield a value of χ_{HF} which is an order of magnitude larger than observed for Fe and Ni, the relative changes of χ_{HF} seem to be very insensitive to the various parameters involved. This is seen in Table IV where the ratios of the susceptibility at 100 kG (or 50 kG) to that at field H_i is tabulated for various values of E_F. Also, for Ni, the rather extreme case of only s-band susceptibility contributions is examined, and again these ratios are not strongly affected by E_F. (The value of $4\pi M_s$ for Ni in Table IV is that part attributed to the slightly polarized s band.) It should be noted that these results for Ni involve densities of states which are also an order of magnitude less than Fe. The ratios $\chi_{HF}(100\text{ kG})/\chi_{HF}(H_i)$ or $\chi_{HF}(50\text{ kG})/\chi_{HF}(H_i)$ are different for Fe and Ni yet these ratios are not strongly dependent on the detailed parameters. This suggests that the relative changes are largely model-independent. [Again we emphasize that we are using a very simple model here and approximate complex band structures (see Figs. 14 and 15) by parabolic bands in order to examine qualitative features of the field-dependent susceptibility. The extent to which these results apply to real metals is very difficult to assess.] Also the average percent deviation of the magnetic moment (up to 250 kG) from the linearly extrapolated moment does not show a strong dependence on the particular parameters. These changes are a few tenths of a percent and not negligible. The magnitudes of the susceptibility ratios are also not small, and in fact, are reasonably close to the observed nonlinear field dependence of the magnetic moment of Fe and Ni. Although we cannot exclude possible systematic errors, we conclude that a nonlinear variation of moment with field, consistent with the experiments, is expected for Fe and Ni.

VI. DISCUSSION AND CONCLUSIONS

Based on reasonable estimates of the orbital contribution (χ_{VV}) to χ, our experiments demonstrate that the occupation of the $3d$ spin bands in Fe and Ni are very different: Fe has holes in both up- and down-spin bands, whereas Ni has one band which is fully occupied. This rather qualitative statement is nevertheless important for our understanding of the origin of ferromagnetism in these metals and the validity of the band or collective electron picture. The simple Stoner expression for χ_d is found to be adequate for describing the results both qualitatively and, as noted, fairly quantitatively despite its total neglect of many-body effects.[1] On the other hand, the band splitting ΔE, or the molecular (exchange) field parameter $k\theta'$ of

[46] E. P. Wohlfarth and P. Rhodes [Phil. Mag. **7**, 1817 (1962)] have discussed the field-dependent susceptibility for an arbitrary state density function for a paramagnetic metal, and D. M. Edwards and E. P. Wohlfarth [Proc. Roy. Soc. (London) **303**, 127 (1968)], have applied this treatment to weakly ferromagnetic metals.

Stoner was seen to be an elusive and difficult quantity to obtain theoretically (as is also the case experimentally). On the other hand, the good agreement obtained by the pseudopotential calculations,[11] which include some correlation effects (Gutzwiller,[42] Hubbard,[43] and Kanamori[44]) is encouraging despite its semiempirical nature.

The extent to which we can compare our present experiments to theory is somewhat limited by the present resolution of band calculations for ferromagnetic metals as well as by the difficulty of estimating more precisely χ_{VV} and the band splitting. The recent developments of Fermi-surface studies and band calculations are quite promising. We expect that as more exact band calculations become available, more quantitative statements will be warranted. It is not possible to assess the magnitude of contributions from many-body effects. Possibly this aspect will be clarified as the band calculations progress.

The experiments discussed in this paper point up several features. It is clear that band contributions to the saturation moment are not negligible for itinerant ferromagnets. These contributions can be measured, but an essential ingredient is the availability of very high magnetic fields. Otherwise, many other contributions, which are unavoidably present at lower fields, cannot be suitably suppressed. The major concern of the static susceptibility measurements involved detailed care with systematic errors; sensitivity of moment measurements was not of great concern here.

Although the microscopic Mössbauer measurements would not at first appear to be appropriate for studies of the field-dependent moment, our results show that this is apparently not so for the special case of Fe. As is often the case with high-resolution microscopic probes,[47] the major problem with the MBE is the lack of knowledge of the functional dependence between the moment and the hyperfine field. If, as is argued, the various competing contributions to H_{int} appear to cancel, a measure of a high-field susceptibility can be obtained from the MBE. In addition, a measure of the nuclear g values is also obtained. The combination of the microscopic Mössbauer measurements and the macroscopic magnetic moment measurements has been extremely valuable for this study as it has been for many other studies of magnetism.

ACKNOWLEDGMENTS

During the course of this study we have profited from discussions and communications from F. M. Mueller, H. Ehrenreich, J. W. D. Connolly, L. Hodges, S. Wakoh, E. P. Wohlfarth, E. D. Thompson, and J. H. M. Stoelinga. We are grateful to A. C. Gossard who first called our attention to important aspects of our Mössbauer studies, and to L. Grodzins for his encouragement and interest in the Mössbauer experiments. We also wish to thank C. Herring, R. M. Bozorth T. R. McGuire, and A. E. Clark for a discussion of their results during an informal meeting at the XIth Conference of Magnetism and Magnetic Materials and for subsequent private discussions. And we would like to thank W. G. Fisher and W. Mosby for their valuable technical assistance during the course of our experiments, and D. Nelson, R. Sheshinsky, and J. Wolf for computer programming.

APPENDIX A: INFLUENCE OF SAMPLE GEOMETRY ON MAGNETIC FIELD DISTRIBUTION

In this appendix we consider the influence of sample geometry on the magnetic field distribution as a function of applied field H_0.[48] In order to simplify the problem we assume that the sample is isotropic and that throughout the sample the magnetic field is large so that the permeability is small. From this assumption it follows that the magnetic moment of the sample is always aligned along the local direction of the magnetic field $\mathbf{B}$ so that

$$\mathbf{B}=\mu_0(\mathbf{H}+\mathbf{m}). \tag{A1}$$

Note that mksa units are used throughout Appendix A.

If we define χ as the paramagnetic contribution to the susceptibility and a function F that has a value equal to one in the sample and zero outside, we can write

$$\mathbf{B}=\mu_0(1+F\chi)\mathbf{H}+\mu_0 m(\mathbf{B}/|\mathbf{B}|), \tag{A2}$$

where μ_0 is the vacuum permeability. This is the region well beyond technical saturation (see Fig. 16). The linearity of this equation shows that we can write

$$\mathbf{B}/|\mathbf{B}|=\mathbf{H}/|\mathbf{H}| \tag{A3}$$

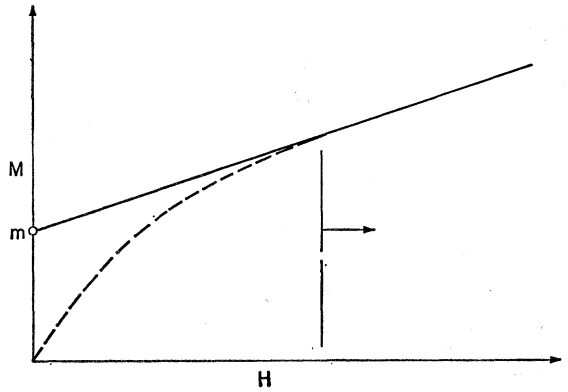

FIG. 16. Sketch showing features of the magnetization M versus H for the sample. The high-field limit (where $\mu \simeq 1$) involves the region to the right of the vertical dashed line.

[47] S. Foner, J. Appl. Phys. 38, 1510 (1967).

[48] R. I. Joseph and E. Schlomann [J. Appl. Phys. 36, 1579 (1965)], have treated this problem for nonellipsoidal bodies. The procedure that we adopt, although not so suitable for quantitative calculations, gives a first-order approximation that goes beyond the approximation scheme those authors use.

as long as

$$1-\mu_0 F(m/|\mathbf{B}|)>0, \tag{A4a}$$

and

$$1+F\chi>0. \tag{A4b}$$

In this case the magnetic field $\mathbf{B}$ is given by

$$\mathbf{B}=\mu_0\mathbf{H}(1+F[\chi+(m/|\mathbf{H}|)]). \tag{A5}$$

For static fields, in a region devoid of currents, we can define a magnetic potential Φ such that

$$H=-\nabla\Phi \tag{A6}$$

and the solution of Maxwell's equation is reduced to the solution of the equation

$$\nabla^2\Phi+\nabla\cdot[F(\chi+m/|\nabla\Phi|)\nabla\Phi]=0. \tag{A7}$$

In the absence of the sample, the scalar potential is given by

$$\Phi_0=-H_0 z, \tag{A8}$$

where we assume the applied magnetic field along the z direction. Therefore, we can write

$$\Phi=-H_0(z+\sum_{n=1}^{\infty} f_n(\mathbf{r})), \tag{A9}$$

where the functions $f_n(\mathbf{r})$ which account for the distortion of the field by the sample should reduce to zero when χ and m are zero. Assuming that the field distortion is small, which is valid if χ and m/H_0 are much smaller than one, then f_1 is the leading correction term which satisfies

$$\nabla^2 f_1+\left(\chi+\frac{m}{H_0}\right)\nabla\cdot\left[F[\hat{e}_z+\nabla f_1]-\frac{(m/H_0)F}{\chi+m/H_0}\hat{e}_z(\hat{e}_z\cdot\nabla f_1)\right]=0. \tag{A10}$$

For Fe and Ni, $m/(\chi H_0)$ is much larger than one even for fields as high as 200 kG; therefore the last term in the curly bracket has a coefficient almost independent of H_0 and very close to 1. In this case the functional dependence of the first-order correction to the magnetic field is

$$f_1(\mathbf{r},\chi,m,H_0)=(\chi+m/H_0)g_1[\mathbf{r},(\chi+m/H_0)]. \tag{A11}$$

Using Eqs. (A5), (A6), (A9), and (A11) and expanding the functions involved up to second order in $(\chi+m/H_0)$. the peak-to-peak output voltage of this series opposing pickup coils is given by

$$V_{pp}=K\mu_0 H_0\{\chi+a(m/H_0)+b(m/H_0)^2\}, \tag{A12}$$

where K, a, and b are constants that take into account the geometry of the coils and the gain of the integrator. We have neglected terms of the form $\chi m/H_0$.

In Eq. (A12), the term am/H_0 is the largest contribution to the output voltage. The first term in the curly bracket gives a contribution of approximately 0.1%; the contribution from the last term is even smaller. However, the curvature introduced by the last term can become quite noticeable particularly if the data is taken for values of m/H_0 not much smaller than one. If we try to fit the data to a straight line, the value of χ will be too large. If the geometry is independent of the magnetic field, the curvature will be such as to decrease the value of χ since the distortion of the magnetic field will decrease with increasing field and the increments in the ouput will be smaller. However, if the equipment is not properly aligned. forces on the sample can make a dependent on the magnetic field, in which case the curvature of the data can vary wildly.

APPENDIX B: RADIAL DISPLACEMENT ERRORS OF A MAGNETIC DIPOLE IN THE PICKUP COILS

We consider the simplified configuration in Fig. 17, where a magnetic dipole D, lies in the plane of a flat coil C, of radius ρ and calculate the magnetic flux change $\Delta\Phi$ when the dipole is displaced by a distance δ from the center of the coil. We assume that $\delta/\rho\ll 1$, since this is closely approximated by the experiments.

To determine the flux enclosed by the coil we integrate over the area complementary to the coil in order to avoid the singularity arising from the assumption of an ideal dipole (since we know that an infinitely large coil will enclose zero flux). The geometry is indicated in Fig. 17 for polar coordinates:

$$\rho^2=\sigma^2+\delta^2-2\sigma\delta\cos\xi,$$

$$\sigma=\delta\cos\xi+(\rho^2-\delta^2\sin^2\xi)^{1/2},$$

and

$$\Phi=c\int_0^{2\pi}d\xi\int_\sigma^\infty\sigma d\sigma\frac{1}{\sigma^3}=c\int_0^{2\pi}\frac{d\xi}{\sigma}\underset{\sim}{\frac{c}{\rho}}\int_0^{2\pi}\frac{d\xi}{1+(\delta/\rho)\cos\xi}$$

$$=-\frac{c}{\rho}\frac{2\pi}{[1-(\delta/\rho)^2]^{1/2}}\approx\frac{2\pi c}{\rho}\left[1+\tfrac{1}{2}\left(\frac{\delta}{\rho}\right)^2\right]\quad\text{for}\frac{\delta}{\rho}\ll 1.$$

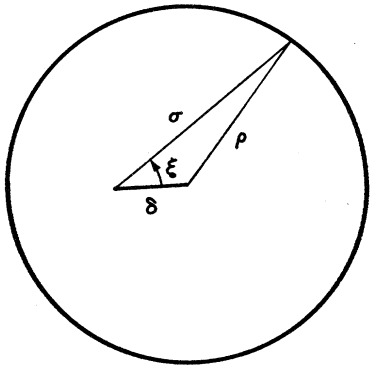

FIG. 17. Polar coordinates for dipole displaced from center of the coil by an amount of δ.

Finally, the error in the integrated flux when the dipole is displaced from the center is given by

$$\epsilon=[\Phi(\delta)-\Phi(0)]/\Phi(0)=\tfrac{1}{2}(\delta/\rho)^2. \quad \text{(B1)}$$

The quadratic dependence is expected from symmetry considerations and the factor $(\frac{1}{2})$ is determined by the particular coil geometry. We expect that this coefficient will not change appreciably for a more realistic coil configuration so that this factor remains near unity. Since we are examining changes of the order of 0.1% in the magnetization of the sample, it is clear that we must have δ/ρ less than about 1%. Coils normally used have inside diameter $\simeq$1 cm so that displacement of less than 0.005 cm must be maintained to keep the error less than 1%.

APPENDIX C: TABULATION OF SPIN-WAVE CONTRIBUTIONS TO THE MAGNETIZATION

In this appendix we have tabulated useful values of the functionals $F_{3/2}$ and $F_{5/2}$ as a function of temperature and field. All the quantities are defined in Sec. III E of the text. The values of applied field H_0 are chosen in increments which are most appropriate to available fields. The smallest intervals of H_0 occur up to 20 kG because these fields are accessible to many iron core magnets. Values of H_0 between 20 and 60 kG are readily attained with superconducting magnets and the larger intervals above 60 kG are available with some superconducting magnets as well as with high-power water-cooled magnets. Fields above 150 kG are much less accessible and progressively larger intervals are tabulated. Three values of temperature are listed 293, 78, and 4.2°K because they are readily available. Values of $F_{3/2}$ and $F_{5/2}$ can be extracted for arbitrary temperature from Table IV when we tabulate these functions only for a wide range of T. In order to ensure convenience and greatest applicability to a wide variety of magnetic materials and experimental conditions we have evaluated quantities which are independent of the material The relative changes with H_0 or T can therefore be examined directly from the tables and the

TABLE V. Tabulation of useful spin-wave functions for $T=293$°K for $5\,\text{kG}\leq H_0\leq 500\,\text{kG}$.

H (kG)	t_H	$1/t_H$	$F_{3/2}(t_H)$	$F_{5/2}(t_H)$	$10^{-3}C_{3/2}$	$10^{-6}C_{5/2}$	$(\partial/\partial T)F_{3/2}$	$(\partial/\partial T)F_{5/2}$	$(\partial/\partial H)F_{3/2}$	$(\partial/\partial H)F_{5/2}$
5	2.297×10^{-3}	4.354×10^{2}	2.446	1.336	4.696	1.464	2.785×10^{-4}	1.917×10^{-5}	-1.632×10^{-5}	-1.123×10^{-6}
6	2.756×10^{-3}	3.628×10^{2}	2.430	1.335	4.666	1.462	3.038×10^{-4}	2.286×10^{-5}	-1.484×10^{-5}	-1.116×10^{-6}
7	3.215×10^{-3}	3.110×10^{2}	2.416	1.333	4.639	1.461	3.270×10^{-4}	2.651×10^{-5}	-1.369×10^{-5}	-1.110×10^{-6}
8	3.675×10^{-3}	2.721×10^{2}	2.403	1.332	4.614	1.460	3.484×10^{-4}	3.014×10^{-5}	-1.276×10^{-5}	-1.104×10^{-6}
9	4.134×10^{-3}	2.419×10^{2}	2.390	1.331	4.590	1.459	3.684×10^{-4}	3.373×10^{-5}	-1.199×10^{-5}	-1.098×10^{-6}
10	4.593×10^{-3}	2.177×10^{2}	2.379	1.330	4.568	1.458	3.871×10^{-4}	3.729×10^{-5}	-1.134×10^{-5}	-1.093×10^{-6}
11	5.053×10^{-3}	1.979×10^{2}	2.368	1.329	4.546	1.456	4.048×10^{-4}	4.083×10^{-5}	-1.078×10^{-5}	-1.088×10^{-6}
12	5.512×10^{-3}	1.814×10^{2}	2.357	1.328	4.526	1.455	4.217×10^{-4}	4.435×10^{-5}	-1.030×10^{-5}	-1.083×10^{-6}
13	5.972×10^{-3}	1.675×10^{2}	2.347	1.327	4.507	1.454	4.377×10^{-4}	4.784×10^{-5}	-9.866×10^{-6}	-1.078×10^{-6}
14	6.431×10^{-3}	1.555×10^{2}	2.337	1.326	4.488	1.453	4.531×10^{-4}	5.130×10^{-5}	-9.483×10^{-6}	-1.074×10^{-6}
16	7.350×10^{-3}	1.361×10^{2}	2.319	1.324	4.453	1.451	4.820×10^{-4}	5.817×10^{-5}	-8.827×10^{-6}	-1.065×10^{-6}
18	8.268×10^{-3}	1.209×10^{2}	2.302	1.322	4.420	1.448	5.089×10^{-4}	6.496×10^{-5}	-8.284×10^{-6}	-1.057×10^{-6}
20	9.187×10^{-3}	1.088×10^{2}	2.286	1.319	4.389	1.446	5.341×10^{-4}	7.168×10^{-5}	-7.824×10^{-6}	-1.050×10^{-6}
25	1.148×10^{-2}	8.708×10^{1}	2.249	1.314	4.319	1.440	5.911×10^{-4}	8.816×10^{-5}	-6.928×10^{-6}	-1.033×10^{-6}
30	1.378×10^{-2}	7.257×10^{1}	2.216	1.309	4.256	1.435	6.416×10^{-4}	1.042×10^{-4}	-6.266×10^{-6}	-1.018×10^{-6}
35	1.608×10^{-2}	6.220×10^{1}	2.186	1.304	4.198	1.429	6.871×10^{-4}	1.200×10^{-4}	-5.752×10^{-6}	-1.004×10^{-6}
40	1.837×10^{-2}	5.442×10^{1}	2.159	1.299	4.145	1.424	7.287×10^{-4}	1.354×10^{-4}	-5.337×10^{-6}	-9.916×10^{-7}
45	2.067×10^{-2}	4.838×10^{1}	2.133	1.294	4.095	1.418	7.670×10^{-4}	1.505×10^{-4}	-4.994×10^{-6}	-9.797×10^{-7}
50	2.297×10^{-2}	4.354×10^{1}	2.109	1.289	4.049	1.413	8.027×10^{-4}	1.653×10^{-4}	-4.704×10^{-6}	-9.686×10^{-7}
55	2.526×10^{-2}	3.958×10^{1}	2.086	1.284	4.005	1.408	8.361×10^{-4}	1.798×10^{-4}	-4.454×10^{-6}	-9.581×10^{-7}
60	2.756×10^{-2}	3.628×10^{1}	2.064	1.280	3.963	1.402	8.675×10^{-4}	1.942×10^{-4}	-4.236×10^{-6}	-9.481×10^{-7}
70	3.215×10^{-2}	3.110×10^{1}	2.024	1.270	3.885	1.392	9.252×10^{-4}	2.221×10^{-4}	-3.873×10^{-6}	-9.259×10^{-7}
80	3.675×10^{-2}	2.721×10^{1}	1.986	1.261	3.814	1.382	9.774×10^{-4}	2.491×10^{-4}	-3.580×10^{-6}	-9.124×10^{-7}
90	4.134×10^{-2}	2.419×10^{1}	1.952	1.252	3.748	1.372	1.025×10^{-3}	2.754×10^{-4}	-3.337×10^{-6}	-8.965×10^{-7}
100	4.593×10^{-2}	2.177×10^{1}	1.919	1.243	3.686	1.362	1.069×10^{-3}	3.009×10^{-4}	-3.132×10^{-6}	-8.817×10^{-7}
110	5.053×10^{-2}	1.979×10^{1}	1.889	1.234	3.627	1.353	1.110×10^{-3}	3.258×10^{-4}	-2.956×10^{-6}	-8.677×10^{-7}
120	5.512×10^{-2}	1.814×10^{1}	1.860	1.226	3.572	1.343	1.148×10^{-3}	3.500×10^{-4}	-2.802×10^{-6}	-8.545×10^{-7}
130	5.972×10^{-2}	1.675×10^{1}	1.833	1.217	3.519	1.334	1.183×10^{-3}	3.736×10^{-4}	-2.667×10^{-6}	-8.420×10^{-7}
140	6.431×10^{-2}	1.555×10^{1}	1.807	1.209	3.469	1.325	1.216×10^{-3}	3.966×10^{-4}	-2.546×10^{-6}	-8.300×10^{-7}
150	6.890×10^{-2}	1.451×10^{1}	1.782	1.201	3.422	1.316	1.248×10^{-3}	4.191×10^{-4}	-2.437×10^{-6}	-8.186×10^{-7}
175	8.039×10^{-2}	1.244×10^{1}	1.724	1.181	3.310	1.294	1.319×10^{-3}	4.730×10^{-4}	-2.208×10^{-6}	-7.919×10^{-7}
200	9.187×10^{-2}	1.088×10^{1}	1.671	1.161	3.209	1.272	1.382×10^{-3}	5.240×10^{-4}	-2.024×10^{-6}	-7.677×10^{-7}
225	1.034×10^{-1}	9.676	1.623	1.142	3.115	1.252	1.437×10^{-3}	5.723×10^{-4}	-1.872×10^{-6}	-7.453×10^{-7}
250	1.148×10^{-1}	8.708	1.577	1.124	3.029	1.232	1.487×10^{-3}	6.182×10^{-4}	-1.743×10^{-6}	-7.246×10^{-7}
275	1.263×10^{-1}	7.916	1.535	1.106	2.948	1.212	1.532×10^{-3}	6.619×10^{-4}	-1.632×10^{-6}	-7.052×10^{-7}
300	1.378×10^{-1}	7.257	1.496	1.089	2.872	1.193	1.572×10^{-3}	7.035×10^{-4}	-1.535×10^{-6}	-6.871×10^{-7}
350	1.608×10^{-1}	6.220	1.423	1.055	2.733	1.156	1.642×10^{-3}	7.809×10^{-4}	-1.375×10^{-6}	-6.537×10^{-7}
400	1.837×10^{-1}	5.442	1.358	1.023	2.607	1.121	1.701×10^{-3}	8.514×10^{-4}	-1.246×10^{-6}	-6.237×10^{-7}
450	2.067×10^{-1}	4.838	1.298	9.927×10^{-1}	2.493	1.088	1.750×10^{-3}	9.158×10^{-4}	-1.139×10^{-6}	-5.963×10^{-7}
500	2.297×10^{-1}	4.354	1.243	9.635×10^{-1}	2.388	1.056	1.791×10^{-3}	9.747×10^{-4}	-1.050×10^{-6}	-5.712×10^{-7}

TABLE VI. Tabulation of useful spin-wave functions for $T=78°K$ for $5\,kG \leq H_0 \leq 500\,kG$.

H (kG)	t_H	$1/t_H$	$F_{3/2}(t_H)$	$F_{5/2}(t_H)$	$10^{-2}C_{3/2}$	$10^{-4}C_{5/2}$	$10^{-3}(\partial/\partial T)F_{3/2}$	$(\partial/\partial T)F_{5/2}$	$(\partial/\partial H)F_{3/2}$	$(\partial/\partial H)F_{3/2}$
5	8.628×10^{-3}	1.159×10^{-2}	2.296	1.321	6.055	5.292	1.949	2.539×10^{-4}	-3.041×10^{-5}	-3.961×10^{-6}
6	1.035×10^{-2}	9.659×10^{-1}	2.267	1.317	5.978	5.276	2.119	3.009×10^{-4}	-2.754×10^{-5}	-3.911×10^{-6}
7	1.208×10^{-2}	8.279×10^{-1}	2.240	1.313	5.909	5.261	2.272	3.469×10^{-4}	-2.531×10^{-5}	-3.866×10^{-6}
8	1.380×10^{-2}	7.244×10^{-1}	2.216	1.309	5.844	5.245	2.412	3.922×10^{-4}	-2.352×10^{-5}	-3.824×10^{-6}
9	1.553×10^{-2}	6.439×10^{-1}	2.193	1.305	5.784	5.230	2.542	4.367×10^{-4}	-2.203×10^{-5}	-3.784×10^{-6}
10	1.726×10^{-2}	5.795×10^{-1}	2.172	1.302	5.728	5.215	2.663	4.805×10^{-4}	-2.077×10^{-5}	-3.748×10^{-6}
11	1.898×10^{-2}	5.269×10^{-1}	2.152	1.298	5.675	5.200	2.776	5.236×10^{-4}	-1.969×10^{-5}	-3.713×10^{-6}
12	2.071×10^{-2}	4.829×10^{-1}	2.132	1.294	5.624	5.185	2.883	5.661×10^{-4}	-1.874×10^{-5}	-3.680×10^{-6}
13	2.243×10^{-2}	4.458×10^{-1}	2.114	1.290	5.576	5.171	2.985	6.080×10^{-4}	-1.791×10^{-5}	-3.648×10^{-6}
14	2.416×10^{-2}	4.140×10^{-1}	2.097	1.287	5.529	5.156	3.081	6.493×10^{-4}	-1.717×10^{-5}	-3.618×10^{-6}
16	2.761×10^{-2}	3.622×10^{-1}	2.064	1.280	5.442	5.127	3.261	7.304×10^{-4}	-1.590×10^{-5}	-3.561×10^{-6}
18	3.106×10^{-2}	3.220×10^{-1}	2.033	1.273	5.361	5.099	3.426	8.095×10^{-4}	-1.485×10^{-5}	-3.508×10^{-6}
20	3.451×10^{-2}	2.898×10^{-1}	2.004	1.266	5.286	5.071	3.578	8.867×10^{-4}	-1.396×10^{-5}	-3.458×10^{-6}
25	4.314×10^{-2}	2.318×10^{-1}	1.939	1.249	5.114	5.003	3.917	1.072×10^{-3}	-1.222×10^{-5}	-3.346×10^{-6}
30	5.177×10^{-2}	1.932×10^{-1}	1.881	1.232	4.961	4.937	4.208	1.248×10^{-3}	-1.094×10^{-5}	-3.246×10^{-6}
35	6.039×10^{-2}	1.656×10^{-1}	1.829	1.216	4.824	4.873	4.463	1.416×10^{-3}	-9.947×10^{-6}	-3.156×10^{-6}
40	6.902×10^{-2}	1.449×10^{-1}	1.781	1.201	4.698	4.810	4.690	1.576×10^{-3}	-9.146×10^{-6}	-3.074×10^{-6}
45	7.765×10^{-2}	1.288×10^{-1}	1.737	1.185	4.582	4.750	4.894	1.729×10^{-3}	-8.483×10^{-6}	-2.998×10^{-6}
50	8.628×10^{-2}	1.159×10^{-1}	1.696	1.171	4.474	4.690	5.079	1.876×10^{-3}	-7.923×10^{-6}	-2.927×10^{-6}
55	9.490×10^{-2}	1.054×10^{-1}	1.658	1.156	4.373	4.632	5.247	2.017×10^{-3}	-7.442×10^{-6}	-2.861×10^{-6}
60	1.035×10^{-1}	9.659	1.622	1.142	4.277	4.576	5.402	2.153×10^{-3}	-7.022×10^{-6}	-2.798×10^{-6}
70	1.208×10^{-1}	8.279	1.555	1.115	4.102	4.466	5.675	2.408×10^{-3}	-6.323×10^{-6}	-2.684×10^{-6}
80	1.380×10^{-1}	7.244	1.495	1.088	3.943	4.360	5.909	2.646×10^{-3}	-5.761×10^{-6}	-2.579×10^{-6}
90	1.553×10^{-1}	6.439	1.440	1.063	3.797	4.259	6.111	2.866×10^{-3}	-5.296×10^{-6}	-2.484×10^{-6}
100	1.726×10^{-1}	5.795	1.389	1.039	3.663	4.161	6.287	3.072×10^{-3}	-4.904×10^{-6}	-2.396×10^{-6}
110	1.898×10^{-1}	5.269	1.341	1.015	3.538	4.067	6.441	3.264×10^{-3}	-4.567×10^{-6}	-2.315×10^{-6}
120	2.071×10^{-1}	4.830	1.297	9.922×10^{-1}	3.421	3.976	6.576	3.444×10^{-3}	-4.275×10^{-6}	-2.238×10^{-6}
130	2.243×10^{-1}	4.458	1.256	9.702×10^{-1}	3.312	3.888	6.695	3.612×10^{-3}	-4.017×10^{-6}	-2.167×10^{-6}
140	2.416×10^{-1}	4.140	1.217	9.489×10^{-1}	3.209	3.802	6.799	3.769×10^{-3}	-3.788×10^{-6}	-2.100×10^{-6}
150	2.588×10^{-1}	3.864	1.180	9.282×10^{-1}	3.112	3.719	6.891	3.916×10^{-3}	-3.583×10^{-6}	-2.036×10^{-6}
175	3.020×10^{-1}	3.312	1.096	8.792×10^{-1}	2.891	3.523	7.072	4.243×10^{-3}	-3.152×10^{-6}	-1.891×10^{-6}
200	3.451×10^{-1}	2.898	1.022	8.335×10^{-1}	2.695	3.340	7.198	4.520×10^{-3}	-2.807×10^{-6}	-1.763×10^{-6}
225	3.882×10^{-1}	2.576	9.551×10^{-1}	7.909×10^{-1}	2.519	3.169	7.282	4.754×10^{-3}	-2.524×10^{-6}	-1.648×10^{-6}
250	4.314×10^{-1}	2.318	8.951×10^{-1}	7.510×10^{-1}	2.361	3.009	7.331	4.950×10^{-3}	-2.287×10^{-6}	-1.544×10^{-6}
275	4.745×10^{-1}	2.107	8.405×10^{-1}	7.136×10^{-1}	2.217	2.859	7.351	5.113×10^{-3}	-2.085×10^{-6}	-1.450×10^{-6}
300	5.177×10^{-1}	1.932	7.906×10^{-1}	6.784×10^{-1}	2.085	2.718	7.348	5.247×10^{-3}	-1.910×10^{-6}	-1.364×10^{-6}
350	6.039×10^{-1}	1.656	7.025×10^{-1}	6.141×10^{-1}	1.853	2.461	7.286	5.440×10^{-3}	-1.624×10^{-6}	-1.212×10^{-6}
400	6.902×10^{-1}	1.449	6.272×10^{-1}	5.568×10^{-1}	1.654	2.231	7.168	5.550×10^{-3}	-1.398×10^{-6}	-1.082×10^{-6}
450	7.765×10^{-1}	1.288	5.620×10^{-1}	5.056×10^{-1}	1.482	2.026	7.011	5.595×10^{-3}	-1.215×10^{-6}	-9.698×10^{-7}
500	8.628×10^{-1}	1.159	5.052×10^{-1}	4.596×10^{-1}	1.332	1.842	6.824	5.588×10^{-3}	-1.065×10^{-6}	-8.717×10^{-7}

TABLE VII. Tabulation of useful spin-wave functions for $T=4.2°K$ for $5\,kG \leq H_0 \leq 500\,kG$.

H (kG)	t_H	$1/t_H$	$F_{3/2}(t_H)$	$F_{5/2}(t_H)$	$C_{3/2}$	$C_{5/2}$	$(\partial/\partial T)F_{3/2}$	$(\partial/\partial T)F_{3/2}$	$(\partial/\partial H)F_{3/2}$	$(\partial/\partial H)F_{5/2}$
5	1.602×10^{-1}	6.241	1.425	1.056	4.695	2.846×10	1.145×10^{-1}	5.435×10^{-2}	-9.616×10^{-5}	-4.566×10^{-5}
6	1.923×10^{-1}	5.201	1.335	1.012	4.399	2.727×10	1.200×10^{-1}	6.111×10^{-2}	-8.400×10^{-5}	-4.278×10^{-5}
7	2.243×10^{-1}	4.458	1.256	9.702×10^{-1}	4.138	2.616×10	1.243×10^{-1}	6.707×10^{-2}	-7.460×10^{-5}	-4.024×10^{-5}
8	2.564×10^{-1}	3.901	1.185	9.311×10^{-1}	3.905	2.510×10	1.277×10^{-1}	7.234×10^{-2}	-6.706×10^{-5}	-3.798×10^{-5}
9	2.884×10^{-1}	3.467	1.121	8.942×10^{-1}	3.695	2.411×10	1.304×10^{-1}	7.700×10^{-2}	-6.085×10^{-5}	-3.593×10^{-5}
10	3.205×10^{-1}	3.121	1.063	8.592×10^{-1}	3.503	2.316×10	1.325×10^{-1}	8.111×10^{-2}	-5.563×10^{-5}	-3.407×10^{-5}
11	3.525×10^{-1}	2.837	1.010	8.260×10^{-1}	3.327	2.227×10	1.340×10^{-1}	8.475×10^{-2}	-5.117×10^{-5}	-3.236×10^{-5}
12	3.845×10^{-1}	2.600	9.606×10^{-1}	7.944×10^{-1}	3.165	2.142×10	1.351×10^{-1}	8.795×10^{-2}	-4.730×10^{-5}	-3.078×10^{-5}
13	4.166×10^{-1}	2.400	9.150×10^{-1}	7.644×10^{-1}	3.015	2.061×10	1.359×10^{-1}	9.076×10^{-2}	-4.390×10^{-5}	-2.932×10^{-5}
14	4.486×10^{-1}	2.229	8.726×10^{-1}	7.358×10^{-1}	2.876	1.983×10	1.363×10^{-1}	9.321×10^{-2}	-4.090×10^{-5}	-2.796×10^{-5}
16	5.127×10^{-1}	1.950	7.961×10^{-1}	6.823×10^{-1}	2.623	1.839×10	1.365×10^{-1}	9.718×10^{-2}	-3.583×10^{-5}	-2.551×10^{-5}
18	5.768×10^{-1}	1.734	7.287×10^{-1}	6.335×10^{-1}	2.401	1.708×10	1.358×10^{-1}	1.001×10^{-1}	-3.169×10^{-5}	-2.335×10^{-5}
20	6.409×10^{-1}	1.560	6.689×10^{-1}	5.888×10^{-1}	2.204	1.587×10	1.345×10^{-1}	1.021×10^{-1}	-2.824×10^{-5}	-2.143×10^{-5}
25	8.011×10^{-1}	1.248	5.450×10^{-1}	4.920×10^{-1}	1.796	1.326×10	1.293×10^{-1}	1.040×10^{-1}	-2.171×10^{-5}	-1.747×10^{-5}
30	9.614×10^{-1}	1.040	4.485×10^{-1}	4.127×10^{-1}	1.478	1.112×10	1.223×10^{-1}	1.027×10^{-1}	-1.712×10^{-5}	-1.437×10^{-5}
35	1.122	8.916×10^{-1}	3.718×10^{-1}	3.472×10^{-1}	1.225	9.359	1.145×10^{-1}	9.928×10^{-2}	-1.374×10^{-5}	-1.191×10^{-5}
40	1.282	7.802×10^{-1}	3.098×10^{-1}	2.927×10^{-1}	1.021	7.892	1.063×10^{-1}	9.455×10^{-2}	-1.116×10^{-5}	-9.928×10^{-6}
45	1.442	6.935×10^{-1}	2.592×10^{-1}	2.473×10^{-1}	8.542×10^{-1}	6.667	9.806×10^{-2}	8.900×10^{-2}	-9.152×10^{-6}	-8.307×10^{-6}
50	1.602	6.241×10^{-1}	2.176×10^{-1}	2.092×10^{-1}	7.171×10^{-1}	5.640	8.998×10^{-2}	8.301×10^{-2}	-7.558×10^{-6}	-6.973×10^{-6}
55	1.762	5.674×10^{-1}	1.831×10^{-1}	1.772×10^{-1}	6.035×10^{-1}	4.776	8.220×10^{-2}	7.685×10^{-2}	-6.277×10^{-6}	-5.868×10^{-6}
60	1.923	5.201×10^{-1}	1.544×10^{-1}	1.502×10^{-1}	5.089×10^{-1}	4.049	7.480×10^{-2}	7.070×10^{-2}	-5.236×10^{-6}	-4.949×10^{-6}
70	2.243	4.458×10^{-1}	1.104×10^{-1}	1.082×10^{-1}	3.636×10^{-1}	2.917	6.134×10^{-2}	5.894×10^{-2}	-3.680×10^{-6}	-3.536×10^{-6}
80	2.564	3.901×10^{-1}	7.922×10^{-2}	7.811×10^{-2}	2.610×10^{-1}	2.106	4.975×10^{-2}	4.835×10^{-2}	-2.612×10^{-6}	-2.538×10^{-6}
90	2.884	3.467×10^{-1}	5.705×10^{-2}	5.647×10^{-2}	1.880×10^{-1}	1.522	3.998×10^{-2}	3.917×10^{-2}	-1.866×10^{-6}	-1.828×10^{-6}
100	3.205	3.121×10^{-1}	4.117×10^{-2}	4.087×10^{-2}	1.357×10^{-1}	1.102	3.188×10^{-2}	3.141×10^{-2}	-1.339×10^{-6}	-1.319×10^{-6}
110	3.525	2.837×10^{-1}	2.976×10^{-2}	2.961×10^{-2}	9.808×10^{-2}	7.982×10^{-1}	2.525×10^{-2}	2.498×10^{-2}	-9.640×10^{-7}	-9.538×10^{-7}
120	3.845	2.600×10^{-1}	2.154×10^{-2}	2.146×10^{-2}	7.099×10^{-2}	5.785×10^{-1}	1.987×10^{-2}	1.972×10^{-2}	-6.956×10^{-7}	-6.903×10^{-7}
130	4.166	2.400×10^{-1}	1.560×10^{-2}	1.556×10^{-2}	5.141×10^{-2}	4.194×10^{-1}	1.556×10^{-2}	1.548×10^{-2}	-5.027×10^{-7}	-5.000×10^{-7}
140	4.486	2.229×10^{-1}	1.131×10^{-2}	1.128×10^{-2}	3.726×10^{-2}	3.042×10^{-1}	1.213×10^{-2}	1.208×10^{-2}	-3.638×10^{-7}	-3.623×10^{-7}
150	4.807	2.080×10^{-1}	8.198×10^{-3}	8.186×10^{-3}	2.702×10^{-2}	2.207×10^{-1}	9.410×10^{-3}	9.382×10^{-3}	-2.635×10^{-7}	-2.627×10^{-7}
175	5.608	1.783×10^{-1}	3.674×10^{-3}	3.671×10^{-3}	1.211×10^{-2}	9.897×10^{-2}	4.911×10^{-3}	4.905×10^{-3}	-1.179×10^{-7}	-1.177×10^{-7}
200	6.409	1.560×10^{-1}	1.648×10^{-3}	1.647×10^{-3}	5.429×10^{-3}	4.440×10^{-2}	2.516×10^{-3}	2.514×10^{-3}	-5.283×10^{-8}	-5.280×10^{-8}
225	7.210	1.387×10^{-1}	7.392×10^{-4}	7.391×10^{-4}	2.436×10^{-3}	1.993×10^{-2}	1.269×10^{-3}	1.269×10^{-3}	-2.370×10^{-8}	-2.369×10^{-8}
250	8.011	1.248×10^{-1}	3.317×10^{-4}	3.317×10^{-4}	1.093×10^{-3}	8.943×10^{-3}	6.328×10^{-4}	6.328×10^{-4}	-1.063×10^{-8}	-1.063×10^{-8}
275	8.812	1.135×10^{-1}	1.489×10^{-4}	1.489×10^{-4}	4.906×10^{-4}	4.014×10^{-3}	3.124×10^{-4}	3.124×10^{-4}	-4.771×10^{-9}	-4.771×10^{-9}
300	9.614	1.040×10^{-1}	6.682×10^{-5}	6.682×10^{-5}	2.202×10^{-4}	1.801×10^{-3}	1.529×10^{-4}	1.529×10^{-4}	-2.141×10^{-9}	-2.141×10^{-9}
350	1.122×10	8.916×10^{-2}	1.346×10^{-5}	1.346×10^{-5}	4.436×10^{-5}	3.629×10^{-4}	3.594×10^{-5}	3.594×10^{-5}	-4.313×10^{-10}	-4.313×10^{-10}
400	1.282×10	7.801×10^{-2}	2.711×10^{-6}	2.711×10^{-6}	8.935×10^{-6}	7.309×10^{-5}	8.275×10^{-6}	8.275×10^{-6}	-8.689×10^{-11}	-8.689×10^{-11}
450	1.442×10	6.935×10^{-2}	5.462×10^{-7}	5.462×10^{-7}	1.800×10^{-6}	1.472×10^{-5}	1.875×10^{-6}	1.875×10^{-6}	-1.750×10^{-11}	-1.750×10^{-11}
500	1.602×10	6.241×10^{-2}	1.100×10^{-7}	1.100×10^{-7}	3.626×10^{-7}	2.966×10^{-6}	4.197×10^{-7}	4.197×10^{-7}	-3.526×10^{-12}	-3.526×10^{-12}

TABLE VIII. Tabulation of $F_{3/2}$ and $F_{5/2}$ for $10^2 \geq t_H \geq 10^{-3}$ and for $10^{-2} \leq 1/t_H \leq 10^3$.

t_H	$F_{3/2}$	$F_{5/2}$	$1/t_H$	$F_{3/2}$	$F_{5/2}$
100.000	3.720×10^{-44}	3.720×10^{-44}	0.01	3.720×10^{-44}	3.720×10^{-44}
90.000	8.194×10^{-40}	8.194×10^{-40}	0.02	1.929×10^{-22}	1.929×10^{-22}
80.000	1.805×10^{-35}	1.805×10^{-35}	0.03	3.338×10^{-15}	3.338×10^{-15}
70.000	3.975×10^{-31}	3.975×10^{-31}	0.04	1.389×10^{-11}	1.389×10^{-11}
60.000	8.757×10^{-27}	8.757×10^{-27}	0.05	2.061×10^{-9}	2.061×10^{-9}
50.000	1.929×10^{-22}	1.929×10^{-22}	0.06	5.778×10^{-8}	5.778×10^{-8}
40.000	4.248×10^{-18}	4.248×10^{-18}	0.07	6.249×10^{-7}	6.249×10^{-7}
30.000	9.358×10^{-14}	9.358×10^{-14}	0.08	3.727×10^{-6}	3.727×10^{-6}
20.000	2.061×10^{-9}	2.061×10^{-9}	0.09	1.495×10^{-5}	1.495×10^{-5}
10.000	4.540×10^{-5}	4.540×10^{-5}	0.10	4.540×10^{-5}	4.540×10^{-5}
9.000	1.234×10^{-4}	1.234×10^{-4}	0.20	6.754×10^{-3}	6.746×10^{-3}
8.000	3.355×10^{-4}	3.355×10^{-4}	0.30	3.613×10^{-2}	3.590×10^{-2}
7.000	9.122×10^{-4}	9.120×10^{-4}	0.40	8.458×10^{-2}	8.331×10^{-2}
6.000	2.481×10^{-3}	2.480×10^{-3}	0.50	1.423×10^{-1}	1.387×10^{-1}
5.000	6.754×10^{-3}	6.746×10^{-3}	0.60	2.030×10^{-1}	1.957×10^{-1}
4.000	1.844×10^{-2}	1.838×10^{-3}	0.70	2.631×10^{-1}	2.508×10^{-1}
3.000	5.069×10^{-2}	5.023×10^{-3}	0.80	3.211×10^{-1}	3.028×10^{-1}
2.000	1.423×10^{-1}	1.387×10^{-1}	0.90	3.763×10^{-1}	3.511×10^{-1}
1.000	4.284×10^{-1}	3.957×10^{-1}	1.00	4.284×10^{-1}	3.957×10^{-1}
0.900	4.828×10^{-1}	4.412×10^{-1}	2.00	8.105×10^{-1}	6.926×10^{-1}
0.800	5.458×10^{-1}	4.926×10^{-1}	3.00	1.041	8.456×10^{-1}
0.700	6.193×10^{-1}	5.507×10^{-1}	4.00	1.199	9.387×10^{-1}
0.600	7.063×10^{-1}	6.169×10^{-1}	5.00	1.315	1.001
0.500	8.105×10^{-1}	6.926×10^{-1}	6.00	1.406	1.047
0.400	9.382×10^{-1}	7.798×10^{-1}	7.00	1.479	1.081
0.300	1.100	8.813×10^{-1}	8.00	1.540	1.108
0.200	1.315	1.001	9.00	1.592	1.130
0.100	1.636	1.148	10.00	1.636	1.148
0.090	1.679	1.164	20.00	1.892	1.235
0.080	1.726	1.181	30.00	2.014	1.268
0.070	1.776	1.199	40.00	2.088	1.285
0.060	1.831	1.217	50.00	2.140	1.296
0.050	1.892	1.235	60.00	2.179	1.303
0.040	1.962	1.255	70.00	2.209	1.308
0.030	2.042	1.275	80.00	2.234	1.312
0.020	2.140	1.296	90.00	2.255	1.315
0.010	2.272	1.318	100.00	2.272	1.318
0.009	2.289	1.320	200.00	2.369	1.329
0.008	2.307	1.322	300.00	2.413	1.333
0.007	2.326	1.325	400.00	2.439	1.335
0.006	2.347	1.327	500.00	2.457	1.336
0.005	2.369	1.329	600.00	2.470	1.337
0.004	2.394	1.332	700.00	2.480	1.338
0.003	2.423	1.334	800.00	2.489	1.338
0.002	2.457	1.336	900.00	2.496	1.339
0.001	2.502	1.339	1000.00	2.502	1.339

absolute values of these contributions are readily determined when the quantity $a_{3/2}$ (and perhaps $a_{5/2}$) is at hand. Similar tables are available for $T=20.4$, 14, and 1.5°K.[49]

Tables V–VII tabulate the following quantities (for indicated values of T) versus H_0 (kG):

$$t_H=g\mu_B H_0/kT;\ 1/t_H;\ F_{3/2};\ F_{5/2}\quad[\text{see Eq. (9)}];$$
$$C_{3/2}=F_{3/2}T^{3/2}/\zeta_{3/2};\ C_{5/2}=F_{5/2}T^{5/2}/\zeta_{5/2};$$
$$(\partial/\partial T)F_{3/2}=(t_H F_{3/2})/T;$$
$$(\partial/\partial T)F_{5/2}=(t_H F_{5/2})/T;$$
$$(\partial/\partial H)F_{3/2}=-(t_H F_{3/2})/H_0;$$

and

$$(\partial/\partial T)F_{5/2}=-(t_H F_{5/2})/H_0.$$

Table VIII tabulates t_H and $(t_H)^{-1}$ over an extended range. A convenient conversion factor for this table is $k/(g\mu_B)=7430$ when $g=2.000$.

[49] For this supplementary material, order NAPS Document 00329 from ASIS National Auxiliary Publications Service, c/o CCM Information Sciences, Inc., 22 West 34th Street, New York, New York 10001, remitting $1.00 for microfiche or $3.00 for photocopies.